U.S.G.S. Award Number: G20AP00079
Project Dates: 06/01/20 – 05/31/21

Detailed Evaluation of Insightful Liquefaction Ejecta Case Histories for the Canterbury Earthquake Sequence, New Zealand

Zorana Mijic[1], Jonathan D. Bray[2], and Sjoerd van Ballegooy[3]

[1]Ph.D. Candidate, Depart. of Civil and Environmental Eng., Univ. of California, Berkeley
[2]Professor, Depart. of Civil and Environmental Eng., Univ. of California, Berkeley
[3]Technical Director, Tonkin and Taylor, Ltd., Auckland, New Zealand

Principal Investigator:
Professor Jonathan D. Bray
Faculty Chair in Earthquake Engineering Excellence
Department of Civil and Environmental Engineering
University of California, Berkeley
453 Davis Hall, MC-1710
Berkeley, CA 94720-1710
Tel. (510) 642-9843
Fax. (510) 642-7476
jonbray@berkeley.edu
URL: https://ce.berkeley.edu/people/faculty/bray

Final Technical Report

August 31, 2021

U.S.G.S. Award Number: G20AP00079

Detailed Evaluation of Insightful Liquefaction Ejecta Case Histories for the Canterbury Earthquake Sequence, New Zealand

Zorana Mijic, Jonathan D. Bray, and Sjoerd van Ballegooy
University of California, Berkeley
Berkeley, CA 94720-1710

ABSTRACT

Liquefaction ejecta were a key mechanism of liquefaction-induced land damage and light-weight residential house damage during the 2010-2011 Canterbury, New Zealand, earthquake sequence. The extensive, repeated occurrence of liquefaction ejecta in the greater Christchurch area is virtually unprecedented in a modern urban setting. A database of well documented field case histories that can be used to develop a procedure to estimate the settlement due to ejecta does not exist currently. The goal of this study was to document cases of the occurrence and quantity of ejecta and its effects on infrastructure using a comprehensive dataset of thousands of CPTs and boreholes, airborne LiDAR surveys, aerial photographs, and detailed inspection reports for individual properties in Christchurch. Direct measurements of ejecta were not available; hence, the ejecta-induced settlement values for each of the four primary earthquakes of the Canterbury sequence were estimated using both LiDAR-based and photographic-based approaches. The settlement analyses were conducted for 61 sites, resulting in 244 insightful case histories. The four main Canterbury earthquakes generated varying degrees of liquefaction-induced land damage ranging from no ejecta to extreme ejecta. The information related to ground conditions and seismic demand leading to the differing quantities of ejecta-induced settlement during the Canterbury earthquake sequence were also extracted. This unique database of detailed ejecta case histories can be used to investigate the occurrence and effects of ejecta. The data can be used to develop procedures to evaluate when liquefaction ejecta will or will not occur and to estimate the quantity of ejecta in earthquakes.

ACKNOWLEDGEMENTS

This research was primarily supported financially by the U. S. Geological Survey (U.S.G.S.), Department of Interior, under USGS award number G20AP00079. Additional support was provided by the U.S. National Science Foundation through Grant CMMI-1956248 and by the Faculty Chair in Earthquake Engineering Excellence at UC Berkeley. The findings, opinions, and conclusions presented in this paper are those of the authors and do not necessarily reflect the views of the sponsoring bodies. The views and conclusions contained in this document are those of the authors and should not be interpreted as necessarily representing the official policies, either expressed or implied, of the U.S. Government. The authors would also like to extend gratitude to James Russell and Oliver Hay of Tonkin and Taylor, Ltd., New Zealand, for their help on this project.

BIBLIOGRAPHY

[No publications were produced by this research at the time of this report.]

Contents

List of Figures

List of Tables

1. INTRODUCTION

The main objective of the research project was to develop detailed liquefaction ejecta case histories for the four main 2010-2011 Canterbury earthquakes, which are the 4 Sep 2010, 22 Feb 2011, 13 June 2011, and 26 Dec 2011 events (Figure 1 and Table 1). Liquefaction ejecta were a key mechanism of liquefaction-induced land damage and light-weight residential house damage during the CES (Rogers et al. 2015). Yet, no procedure for estimating the occurrence and the amount of ejecta-induced settlement is currently available. There is also no database with detailed case histories that could be used to develop the procedure or gain insights into the complex mechanism of ejecta, ground conditions, and seismic demand leading to the occurrence or non-occurrence of ejecta and the differing degrees of ejecta-induced settlement. The well-documented 2010-2011 Canterbury Earthquake Sequence (CES) represents an unprecedented opportunity for developing the liquefaction ejecta database that can be used as a key resource for examining the occurrence and effects of liquefaction ejecta and as a basis for the development of procedures to evaluate the occurrence of ejecta and the amount of ejecta when it occurs.

The four main Canterbury earthquakes caused widespread liquefaction in Christchurch, New Zealand (NZ). Liquefaction affected 51,000 of 140,000 residential properties, damaging approximately 15,000 properties beyond economic repair (Rogers et al. 2015). The level of infrastructure damage and the occurrence of liquefaction ejecta were strongly correlated (Rogers et al. 2015). Areas without liquefaction ejecta or lateral spreading, although some areas likely had liquefaction at depth, had typically negligible liquefaction-induced land or building damage. Conversely, areas with liquefaction ejecta or lateral spreading had moderate to severe land or building damage (Rogers et al. 2015).

Liquefaction-induced ground deformation has three primary components: (1) shear-induced ground deformation resulting from soil-structure-interaction ratcheting and punching failure, (2) volumetric-induced deformation due to sedimentation and post-liquefaction reconsolidation, and (3) ejecta-induced ground deformation due to the loss of soil ejected onto the ground surface (Bray and Dashti 2014). The shear-induced building settlement can be estimated using the Bray and Macedo (2017) procedure. The volumetric-induced settlement can be estimated using the Zhang et al. (2002) procedure. However, there are not procedures for estimating ejecta-induced ground settlement. The Liquefaction Severity Number, LSN, (van Ballegooy et al. 2014) and Liquefaction potential Index, LPI, (Iwasaki et al. 2012) indices were not developed specifically to estimate the occurrence and amount of liquefaction ejecta.

A database with detailed ejecta case histories that could be used to develop a procedure for estimating when ejecta will occur and how much ejecta-induced free-field settlement will occur does not exist. The well-documented CES and the degree of extensive, repeated liquefaction in Christchurch and its suburbs represent an unparalleled opportunity to study the extent and occurrence of ejecta. Sites throughout Christchurch were shaken multiple times and experienced no-to-extreme quantities of liquefaction ejecta (Figure 2). The degree of liquefaction ejecta-induced damage varied from site to site and from earthquake to earthquake. Although direct measurements of ejecta are not available after the Canterbury earthquakes, liquefaction ejecta coverage and amounts for each of the four major Canterbury earthquakes can be characterized with access to the comprehensive T+T (2015) database. The database contains aerial photographs for each earthquake, pre- and post-earthquake airborne LiDAR surveys, ground surveys, thousands of cone penetration tests (CPTs) and boreholes with installed instruments, robust estimates of PGA with uncertainties, ground photographs, and detailed land damage inspection notes.

Liquefaction ejecta tends to form in the presence of a low-permeability cap above the liquefying sediments (Obermeier 1996). A mixture of water and sediments is typically ejected onto the ground surface through preexisting gaps in the cap or dikes produced by hydraulic fracturing of the cap. The severity of liquefaction manifestation at the ground surface is influenced by the thickness and properties of the cap and the characteristics of the underlying liquefying soil strata. A non-liquefying crust that is thicker than underlying liquefying soil strata tends to reduce the effects of liquefaction at the ground surface (van Ballegooy et al. 2014). Formation of ejecta is also affected by the built environment due to the load applied by infrastructure, disruption of an upward drainage path by an impervious constructed layer which may force the liquefied material to migrate sideways around it, and defects created in the crust, such as from light poles.

The geology of Christchurch has been influenced by alluvial and coastal depositional processes. The complex depositional environment can be divided into four geologic quadrants centered on the Christchurch Business District (CBD) for the assessment of liquefaction performance (Beyzaei et al. 2018). The southwestern highly stratified silty soil swamp deposits with depositional effects from the volcanic complex of the Port Hills of Banks Peninsula had liquefaction manifestation at the ground surface systematically overestimated by state-of-the-practice liquefaction triggering procedures and liquefaction damage indices (e.g., LSN and LPI). The northwestern silty soil swamp deposits have thicker layers of peat than the southwestern part of the city and are more influenced by the Waimakariri River without the depositional effects from the Port Hills. The northeastern and southeastern interlayered deposits of coastal and fluvial sediments, in general, had few discrepancies between liquefaction manifestation estimations and liquefaction observations. The eastern deposits are characterized primarily by thicker layers of clean sand than the western deposits, which comprise most of the case histories database that was used to develop the simplified liquefaction triggering procedures. The presence of a soil stratum that has a lower hydraulic conductivity than a soil stratum below it has the potential to interrupt the communication between layers in their dynamic response and pore water pressure redistribution and impede the propagation of excess pore water pressures toward the ground surface (e.g., Cubrinovski et al. 2019, Hutabarat and Bray 2021). Furthermore, the coastal zone of Christchurch, up to 15 km inland from the present-day coastline, is comprised of gravels interlayered with finer-grained marine/estuarine strata (silt, silty sand, clay, and peat) wherein channelized gravel forms particularly good aquifers and the marine/estuarine sediments act as aquitards (Brown et al. 1995, as cited in Cox et al. 2021).

This report begins with an overview of data that was used to conduct the research and explanation of methodology used to estimate the ejecta-induced settlement and develop detailed ejecta case histories. The methodology is described for two illustrative sites in Christchurch, i.e., Shirley Intermediate School and Tonks St. The Shirley Intermediate School site is predominantly an open field site that manifested ejecta for the Feb 2011, June 2011, and Dec 2011 earthquakes. The 31 Tonks St site is in the residential area and had no ejecta for any earthquake event. Finally, closing remarks regarding the research outcomes and deliverables as well as the guidance for future work are provided.

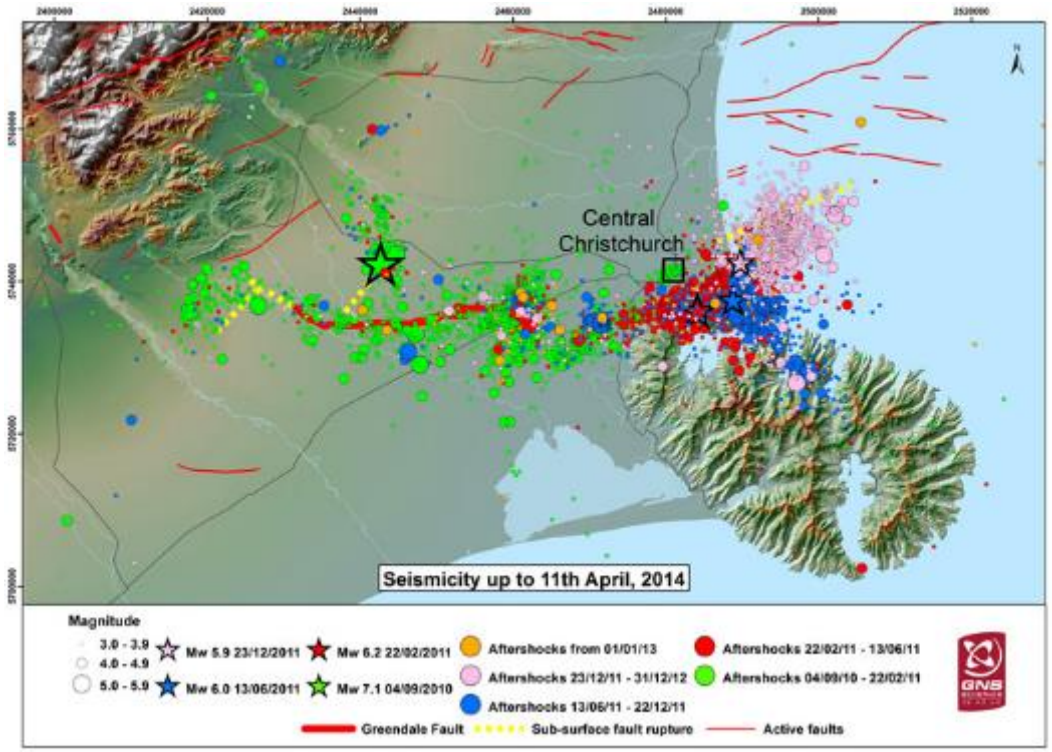

Figure 1: Location of 4 Sep 2010 Darfield main shock and subsequent aftershocks up to 11 Apr 2014 (GNS Science 2021).

Table 1: Event characteristics for Canterbury earthquake sequence

Event	Date	NZ Local Time	M_w (USGS)	Hypocentral Latitude	Hypocentral Longitude	Strike (°)	Dip (°)	Z_{tor} (km)
1	4 Sep 2010	04:35:46	7.1	-43.5382	172.1635	85.1	82.2	0.0
2	22 Feb 2011	12:51:42	6.2	-43.5644	172.6915	50	64	0.5
3a	13 Jun 2011	13:01:00	5.3	-43.568	172.753	--	--	--
3b	13 Jun 2011	14:20:50	6.0	-43.5638	172.7431	162	67	1.41
4a	23 Dec 2011	12:58:36	5.8	-43.4862	172.7957	45	63	0.0
4b	23 Dec 2011	14:18:02	5.9	-43.5300	172.7428	57	51	1.47

Notes:

1) Moment magnitudes were retrieved from GeoNet (www.geonet.org.nz) regional Centroid Moment Tensor (CMT) solutions (Ristau 2008).
2) Strike, dip, and Z_{tor} values are based on Metadata received from Bradley (2013) via personal communication, except for the 22 Feb 2011 event; the 22 Feb 2011 values are based on Bradley and Cubrinovski (2011).
3) Hypocentral latitude and longitude for Event 3a were obtained from Quigley et al. (2016).

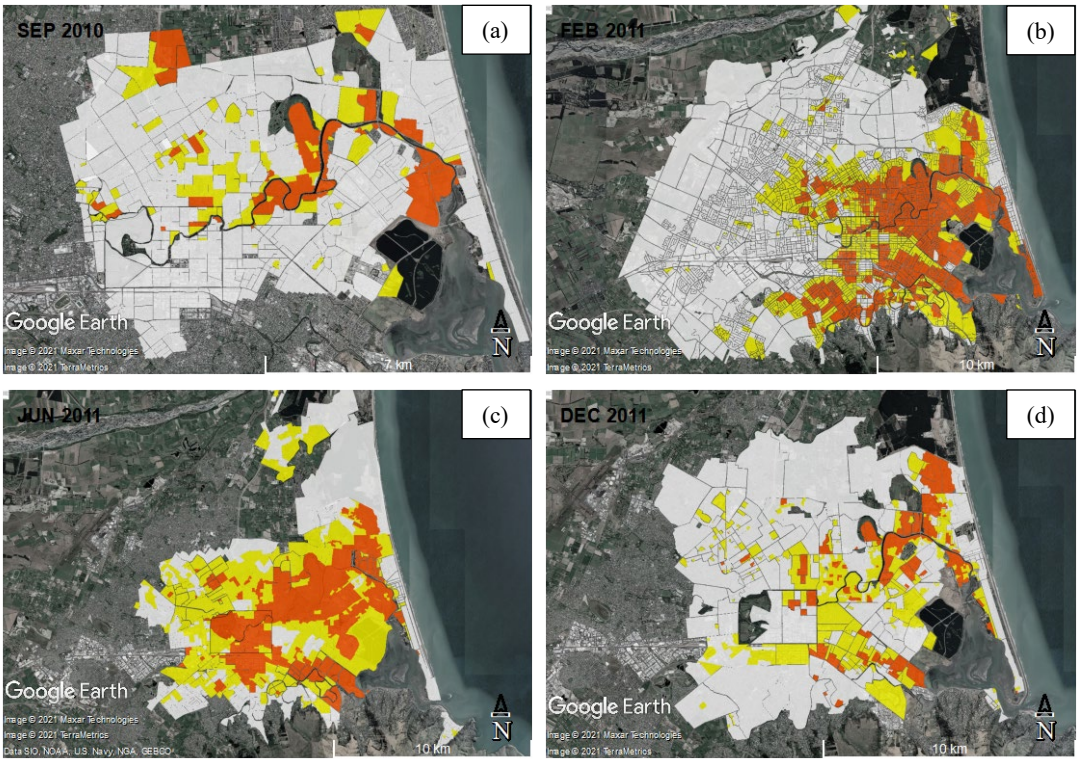

Figure 2: Liquefaction observations at the ground surface for the (a) 4 Sep 2010, (b) 22 Feb 2011, (c) 13 Jun 2011, and (d) 23 Dec 2011 earthquakes *(CGD 2013a)*. Legend: orange = moderate-to-severe liquefaction manifestation, yellow = minor-to-moderate liquefaction manifestation; white = no liquefaction observations.

2. DATA, MATERIALS, AND METHODOLOGY

2.1 Data and Materials Available

The scale and extent of land damage caused by the four main Canterbury earthquakes and having land insured for natural disaster damage in NZ under the 1993 Earthquake Commission (EQC) Act resulted in a comprehensive geotechnical land damage assessment across Christchurch and its suburbs. The initial assessment of the extent and severity of land damage through regional-scale mapping and rapid property-by-property mapping identified the areas that needed detailed EQC Land Damage Assessment Team (LDAT) inspection of individual properties (T+T 2013). Following the detailed inspection of liquefaction-induced land damage at approximately 65,000 properties by assessment teams, over 25,000 cone penetration tests (CPTs), over 5,000 boreholes, many with piezometers installed, and several kilometers of geophysical surveys were conducted in the greater Christchurch area.

2.1.1 Airborne LiDAR Surveys

Airborne Light Detection And Ranging (LiDAR) surveys of Christchurch were conducted before and after each of the four main 2010-2011 Canterbury earthquake events to estimate the ground surface subsidence caused by each earthquake. The surveys of areas with significant liquefaction and tectonic movement were acquired by AAM Brisbane (AAM) Pty and New Zealand Aerial Mapping (NZAM) Ltd. on (1) 6-9 JUL 2003, (2) 5 SEP 2010, (3) 8-10 MAR 2011, (4) 20-30 MAY 2011, (5) 18 and 20 JUL, 11 AUG, 25-27 AUG, and 2-3 SEP 2011 (Russell and van Ballegooy 2015), and (6) 25 OCT 2015. Thus, each LiDAR survey, apart from the Sep 2010 LiDAR survey, was flown at least a month after each main earthquake when much of liquefaction ejecta were removed from most properties and roads. The position data points were acquired as a LiDAR survey point cloud and were classified as ground points or points that reflected off vegetation and structures (non-ground points). The accuracy of the acquired LiDAR points was verified against elevations of the Land Information New Zealand (LINZ) benchmarks that were surveyed using GPS-based equipment and precise levelling (Russell and van Ballegooy 2015). Low mean and median approximate errors suggest reasonable overall accuracy. Approximately 80% of the LiDAR point elevations for all post-Sep 2010 LiDAR surveys have a vertical accuracy of ±70 mm. A vertical accuracy of the July 2003 LiDAR points is lower as approximately 80% of the LiDAR point elevations are within ±150 mm. The lower accuracy is likely due to the lower density of LiDAR points and lower precision in the LiDAR equipment in 2003 (Russell and van Ballegooy 2015).

The ground classified points were also used to develop the bare earth digital elevation models (DEMs) that consist typically of 5 m by 5 m cells (Russell and van Ballegooy 2015). Each cell represents an average ground surface elevation obtained by averaging the ground classified points within the DEM cell (Russell and van Ballegooy 2015). The difference between a pre-earthquake DEM and a post-earthquake DEM can be used to estimate the change in vertical ground surface elevation due to an earthquake. However, there are limitations to estimating the ground surface subsidence from a difference DEM. The limitations include a localized error due to the interpolation of adjacent DEM cell elevations in areas with vegetation and buildings thus fewer ground classified points and the difference between the actual ground surface elevation and the average DEM elevation in areas with step changes in the ground surface (Russell and van

Ballegooy 2015). The difference DEMs can also be used to identify areas of greater uplift or subsidence due to anthropogenic changes (e.g., construction and vegetation removal) and error bands of apparent greater subsidence that are centered on and are parallel to individual LiDAR flight paths. These error bands are the artefacts of the LiDAR point acquisition and the post-acquisition processing that involves a combination of automated and manual classification of non-ground classified points. Detailed explanation of the accuracy and limitations of the DEMs and the LiDAR points is provided in Russell and van Ballegooy (2015).

2.1.2 Aerial Photography

High-resolution aerial photographs of Christchurch and its suburbs were acquired by NZAM after each main Canterbury earthquake – 5 SEP 2010, 24 FEB 2011, 14-15 JUN 2011, 16 JUN 2011, and 24 DEC 2011 – to identify areas with liquefaction ejecta to which inspection teams were dispatched to map the induced damage. They were supplied as orthorectified, color-balanced, geolocated, tiled images and were transformed into image pyramids for efficient use (CGD 2013a). The image locations may have some inaccuracy because the locations of the reference datums used during acquisition were not verified at the time of supply, in addition to an approximate, average 1-m residual error that stems from the orthorectification process (CGD 2013a).

2.1.3 Detailed LDAT Property Inspection Mapping

About 65,000 properties in Christchurch and its suburbs were visually inspected in detail for liquefaction-related land damage to resolve the EQC land damage insurance claims (T+T 2013). The inspection of individual properties was performed by the EQC LDAT comprised of approximately 400 geotechnical engineers and engineering geologists (T+T 2013). The LDAT used a land damage template form to collect land damage information: lateral spreading, cracks, undulating land, local ponding, localized settlement causing drainage issues, new groundwater springs, and inundation of land with ejected soil. They also identified damage to any sloping land, retaining wall, foundation, and dwelling. Additionally, the LDAT used a property map with a recent aerial photograph to sketch locations of observed damage for each individual property. It is worth noting that liquefaction ejecta were often removed or eroded at the time of inspection, which makes the high-resolution aerial photographs an important supplement in assessing the extent of ejecta. The LDAT took photographs of ejecta remnants, sketched their approximate locations on individual property maps, and often reported the maximum height of ejecta remnants. In some cases, claimants provided useful information regarding ejecta and its volume/height.

2.1.4 Conditional PGA

Robust estimates of conditional Peak Ground Accelerations (PGAs) were developed for site-specific assessment of liquefaction due to each main Canterbury earthquake as a combination of an empirical ground motion prediction model and recordings at 19 strong motion stations within the Canterbury region (Bradley and Hughes 2012). The conditional PGA at each location was defined probabilistically in terms of its median value and uncertainty (lognormal standard deviation). The accuracy of the predicted PGA decreases with the increasing distance from strong

motion stations and increases with the increasing proximity to the strong motion stations. For site locations that are far from the strong motion stations, the conditional distribution of PGA is similar to the unconditional distribution of PGA. For sites close to the strong motion stations, the conditional distribution approaches the PGA value recorded at the station (Bradley and Hughes 2012). The PGAs are available in the form of contour maps (CGD 2015b).

2.1.5 Event-Specific Groundwater Table Depths

The event-specific groundwater depths are based on water level measurements from wells installed prior to and after the SEP 2010 earthquake and the most appropriate LiDAR-derived DEM (CGD 2014). Groundwater levels in the wells were converted to free surface elevations based on surveyed wellhead levels. The elevations at the wells and the adjacent rivers prior to each main Canterbury earthquake were used to develop surface models that were subtracted from the corresponding LiDAR DEM. The obtained groundwater depths are based on the mean free surface elevations at the time of each earthquake. In case of geographical sparsity of wells for earlier earthquakes, water level measurements at the newly installed wells were used to extrapolate the free surface elevations back in time. The fitted surface models for each earthquake are color-banded and available as an image pyramid (CGD 2014).

2.2 Sites used for the development of case histories

The US-NZ researchers developed a comprehensive dataset of 55 Christchurch sites to investigate liquefaction triggering aspects in detail. The dataset includes field observations, measurement data, and field data. It consists predominantly of sites that were not well captured by state-of-the-practice liquefaction triggering procedures, i.e., liquefaction ejecta did not occur even though severe manifestation of liquefaction at the ground surface was estimated. This dataset is, therefore, biased toward cases with none to minor ejecta. The "55 sites" data is discussed in Russell and van Ballegooy (2015) and Stewart et al. (2015), and is used in several research papers (e.g., Cubrinovski et al. 2017). In this study, 20 sites of the "55 sites" were not used to develop detailed ejecta case histories typically due to lateral spreading, many topographical features, and ejecta that were not recognizable in the aerial photographs but the property inspection reports suggested their occurrence. There are also eight of these sites for which only coarse analyses were performed and the best final estimates of the free-field ejecta-induced settlement were reported. They had no to minor ejecta, no LiDAR surveys, or one CPT only. Thus, 27 sites of the "55 sites" database were investigated in detail in this study. Each site and the pertinent information are provided in the EjectaCaseHistories_FlatFile_2021.xlsx spreadsheet, an electronic supplement to this report.

An additional 34 sites, primarily from the NE quadrant of Christchurch, were selected to form an unbiased database. These were high-quality sites with good observations (i.e., aerial and ground photographs and EQC LDAT property inspection reports), reliable settlement estimates based on the LiDAR survey data, at least two closely spaced CPTs with investigation depths of 15-20 m, a nearby borehole, and without significant discrepancies between liquefaction observations and liquefaction manifestation estimations as per state-of-the-practice liquefaction triggering procedures and corresponding liquefaction damage indices. It is worth noting that the LiDAR error bands could not always be avoided because large amounts of ejecta were sometimes present at a site with good photographic evidence and detailed property inspection reports.

The newly developed 34 sites and the 27 sites from the "55 sites" dataset were used to build 244 detailed case histories (i.e., 61 sites times four earthquakes). Figure 3 illustrates the site locations, while Table 2 lists the occurrence of ejecta for each earthquake event. All details related to the case histories are provided in the Appendix. The important information related to each site and each earthquake is provided in the EjectaCaseHistories_FlatFile_2021.xlsx spreadsheet.

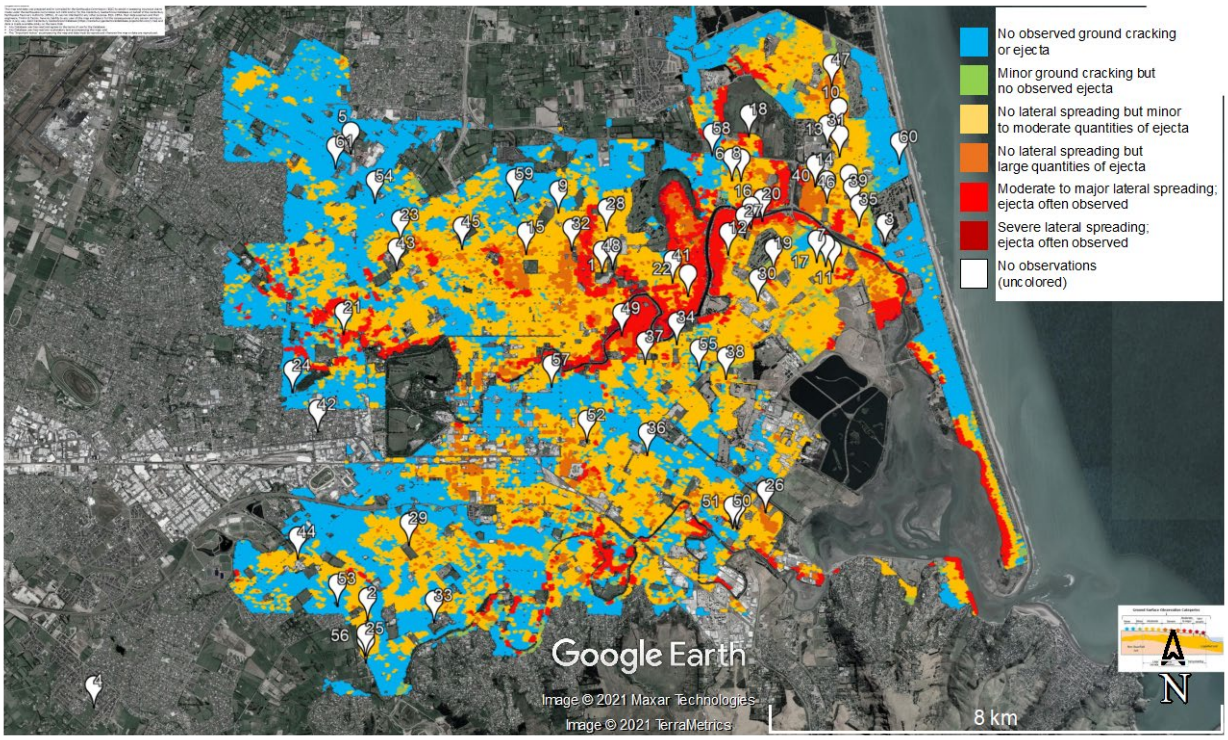

Figure 3: Liquefaction ejecta-induced damage map for the Feb 2011 earthquake *(CGD 2013b)* with site locations. (The site numbers match the site order in the appended documents.)

Table 2: Locations and general characteristics of sites analyzed for ejecta-induced settlement.

Site Name	Site ID	Long. [deg]	Lat. [deg]	Quad-rant	Site Type	Ejecta Occurrence			
						Sep 2010 EQ	Feb 2011 EQ	Jun 2011 EQ	Dec 2011 EQ
Shirley Intermediate School	VsVp 57203	172.661995	-43.510408	NE	Open field	No	Yes	Yes	Yes
Rydal Reserve	VsVp 57190	172.608493	-43.565806	SW	Open field + residential area	Yes	Yes	No	No
Rawhiti Domain	VsVp 57188	172.721404	-43.506685	NE	Open field + residential area	No	No	No	No
Caulfield Ave	VsVp 38175	172.548658	-43.579706	SW	Open field	Yes	No	No	No

Site Name	Site ID	Long. [deg]	Lat. [deg]	Quad-rant	Site Type	Ejecta Occurrence			
						Sep 2010 EQ	Feb 2011 EQ	Jun 2011 EQ	Dec 2011 EQ
70 Langdons Rd	VsVp 57142	172.604872	-43.492195	NW	Open field	No	No	No	No
Vivian St	CPT 5586	172.689983	-43.496445	NE	Residential area	No	Yes	Yes	Yes
50 Eureka St	VsVp 57195	172.706500	-43.509273	NE	Residential area	No	Yes	Yes	No
Parnwell St & Bassett St	CPT 27709	172.687992	-43.496341	NE	Residential area	No	Yes	Yes	Yes
Vangelis Ln & Fernbrook Pl	CPT 49582	172.650158	-43.501489	NE	Open field + residential area	No	Yes	No	Yes
Pinewood Ave	CPT 61991	172.711272	-43.488333	NE	Residential area	No	Yes	Yes	Yes
Carisbrooke Playground	VsVp 57193	172.709944	-43.510815	NE	Open field + residential area	No	Yes	No	No
Avondale Playground	VsVp 57062	172.687194	-43.508109	NE	Open field + residential area	No	Yes	Yes	No
Bower Ave	CPT 3937	172.711488	-43.492600	NE	Residential area	No	Yes	Yes	Yes
Wattle Dr	CPT 90678	172.706167	-43.497325	NE	Residential area	No	Yes	Yes	Yes
Warrington St	CPT 44959	172.643107	-43.508034	NE	Residential area	Yes	Yes	Yes	Yes
Hunt Ln	CPT 4674	172.692150	-43.503948	NE	Residential area	No	Yes	Yes	Yes
Sandown Cres	CPT 15498	172.708479	-43.509917	NE	Residential area	No	Yes	Yes	No
Travis Country Dr	CPT 29778	172.691683	-43.489401	NE	Residential area	No	Yes	Yes	Yes
Aldershot St	CPT 5261	172.697064	-43.510579	NE	Residential area	No	Yes	Yes	Yes
1/19 Chardale St	VsVp 57320	172.694632	-43.502797	NE	Residential area	Yes	--	--	--
15b Royds Pl	VsVp 57326	172.603276	-43.520686	NW	Residential area	No	--	--	--
31 Landy St (VsVp site moved to CPT)	CPT 44439	172.678436	-43.514681	NE	Residential area	Yes	Yes	Yes	Yes
Normans Rd/Papanui Rd	VsVp 57200	172.615699	-43.506100	NW	Open field + residential area	No	--	--	--
St. Teresa's School	VsVp 57191	172.592135	-43.529873	NW	Urban school/church area	No	No	No	No

Site Name	Site ID	Long. [deg]	Lat. [deg]	Quad-rant	Site Type	Ejecta Occurrence			
						Sep 2010 EQ	Feb 2011 EQ	Jun 2011 EQ	Dec 2011 EQ
Kaiwara Reserve	VsVp 57182	172.608046	-43.571492	SW	Open field + residential area	No	Yes	No	No
Ti Rakau Reserve	VsVp 57186	172.695373	-43.548825	SE	Open field + residential area	No	Yes	Yes	Yes
Avondale Park	VsVp 57187	172.690763	-43.505496	NE	Open field + residential area	No	Yes	Yes	Yes
Sabina Playground	VsVp 57192	172.660660	-43.504340	NE	Open field + residential area	No	Yes	Yes	Yes
Barrington Park	VsVp 38172	172.617541	-43.554035	SW	Open field + residential area	No	Yes	Yes	No
Shortland St	CPT 6551	172.693665	-43.515402	NE	Residential area	No	Yes	Yes	No
Mark Treffers Dr	CPT 62594	172.708784	-43.491115	NE	Open field	No	Yes	Yes	Yes
Shirley Primary School	CPT 54376	172.653071	-43.507478	NE	Open field + school area	No	Yes	Yes	No
Cashmere High School	CPT 33732	172.623013	-43.566259	SW	Open field + school area	No	Yes	No	No
Dunarnan St	CPT 17908	172.675985	-43.522271	NE	Residential area	No	Yes	Yes	Yes
Baker St	CPT 14070	172.715770	-43.503609	NE	Residential area	No	Yes	Yes	Yes
Randolph St	CPT 44440	172.669546	-43.539782	NE	Residential area	No	Yes	Yes	No
Woodham Rd	CPT 25514	172.669086	-43.525337	NE	Residential area	No	Yes	Yes	No
Rudds Rd	CPT 5687	172.686716	-43.527755	NE	Residential area	No	Yes	Yes	No
Palmers Rd	CPT 27040	172.713519	-43.498906	NE	Residential area	No	Yes	Yes	Yes
Willryan Ave	CPT 2168	172.708731	-43.499905	NE	Residential area	No	Yes	Yes	Yes
Bideford Pl	CPT 17200	172.675071	-43.512497	NE	Residential area	Yes	Yes	Yes	No
Wharenui School	VsVp 57165	172.597625	-43.536096	SW	Open field + school area	No	No	No	No

Site Name	Site ID	Long. [deg]	Lat. [deg]	Quad-rant	Site Type	Ejecta Occurrence			
						Sep 2010 EQ	Feb 2011 EQ	Jun 2011 EQ	Dec 2011 EQ
Heaton Normal Intermediate School	VsVp 57181	172.614886	-43.510572	NW	Open field + school area	Yes	Yes	Yes	Yes
Hillmorton High School	VsVp 57201	172.593252	-43.556187	SW	Open field + school area	No	Yes	No	No
St. Albans Catholic School	VsVp 57180	172.629117	-43.507198	NW	Open field + residential area	No	Yes	Yes	No
113A Palmers Rd	CPT 29740	172.714230	-43.500972	NE	Residential area	No	Yes	Yes	Yes
Hurst Pl	CPT 25981	172.709763	-43.481524	NE	Residential area	No	Yes	Yes	Yes
Shirley Boys High School	CPT 56468	172.659684	-43.511008	NE	Open field + residential area	No	Yes	Yes	Yes
Bracken St	CPT 59661	172.663966	-43.520893	NE	Residential area	Yes	Yes	Yes	Yes
Palinurus Rd 1	VsVp 57185	172.688215	-43.551331	SE	Open field	No	No	No	No
Palinurus Rd 2	CPT 62761	172.689145	-43.551414	SE	Open field	No	Yes	Yes	No
Nursery Rd	CPT 17262	172.656360	-43.537748	SE	Open field	No	Yes	Yes	No
Gainsborough Reserve	VsVp 38176	172.601913	-43.563623	SW	Open field	No	No	No	No
455 Papanui Rd	VsVp 57189	172.610136	-43.499954	NW	Open field	No	No	No	No
Keers Rd	CPT 28986	172.680817	-43.526519	NE	Residential area	No	No	No	No
200 Cashmere Rd	VsVp 38171	172.608100	-43.572615	SW	Open field	No	No	No	No
Armagh St	CPT 45795	172.648678	-43.529008	NE	Open field + residential area	No	No	No	No
Lakewood Dr	CPT 54736	172.683682	-43.492444	NE	Residential area	No	No	No	No
Kensington Ave	CPT 88252	172.640665	-43.499634	NE	Residential area	No	No	No	No
Tonks St	CPT 128494	172.7245	-43.493746	NE	Residential area	No	No	No	No
Marblewood Reserve	VsVp 57155	172.601543	-43.494509	NW	Open field + residential area	No	No	No	No

2.3 Methodology

Each site was centered on a CPT or cross-hole shear wave velocity (V_s) survey location and encompassed an area within a 50-m radius of its center (termed a 50-m buffer). The 10-m and 20-m radii (10-m and 20-m buffers, respectively) were used primarily in the analyses due to the spatial variation in ejecta distribution and presence of buildings. A site was first inspected for the presence of free-face features, sloping land, retaining walls, buildings, vegetation, pavement, and anthropogenic changes, which were noted carefully as they could affect liquefaction manifestation at the ground surface and LiDAR survey measurements. This information for each site can be found in Appendix A – Table 1 in each site description. The supporting figures for each site were also included in Appendix A. An area free of vegetation, buildings, anthropogenic changes, and with representative distribution of ejecta for the site was selected for detailed settlement assessment (Appendix A – Figure 1 in each site description).

Two methods for estimating the free-field ejecta-induced settlement were developed. The photographic-based method involved the use of aerial and ground photographs, EQC LDAT property inspection reports and maps, and geometrical approximations of the ejected soil shapes. The second method was based on LiDAR point elevations and one-dimensional, free-field volumetric-induced settlement for level ground as per Zhang et al. (2002). The best final estimate of the ejecta-induced settlement was determined as the weighted average of the two estimates.

The detailed case histories documents are provided in Appendix A. The ejecta-induced settlement estimates based on the two methods and the best final estimates of the ejecta-induced settlement along with other important information, including the soil profile category, PGAs, groundwater table depths, crust thickness, LPI, LSN, ejecta pattern, ejecta distribution, and ejecta quantum (as defined by Russell and van Ballegooy 2015) for each case history, were extracted into the EjectaCaseHistories_FlatFile_2021.xlsx spreadsheet. Based on LSN and LPI and the ejecta quantum, the accuracy of their estimate of liquefaction severity was also provided.

2.2.1 Photographic-based ejecta-induced settlement

To obtain the photographic-based settlement due to ejecta, $S_{E,P}$, the shape of the ejecta manifestations had to be estimated first. Ejecta were shaped typically as a prism with irregular curvilinear bases, prism with triangular bases, isolated and naturally occurring cone, and artificially formed pile as a result of cleaning. The portion of the assessment area covered by ejecta was then quantified. This was done in *Google Earth*^{TM} by outlining the coverage area on the high-resolution aerial photograph for each earthquake. The available photographs, reports, and geometrical approximations were used to estimate the height of ejecta.

For ejecta shaped as a prism with irregular curvilinear bases (Figure 4), the differing thicknesses of ejecta were identified on the high-resolution aerial photographs as having different colors (i.e., darker colors were assumed to correspond to thicker ejecta layers because of the longer time required to dry the soil) and the corresponding areas were measured using a polygon tool. The height of each ejecta layer was estimated based on the available ground photographs, LDAT property inspection maps, reports that occasionally included the height of ejecta remnants, visibility of the ejecta layer in the aerial photographs (e.g., the upper estimate of height of ejecta that were barely visible in the aerial photographs did not exceed 50 mm), and measurements of the ejecta height in neighboring, similarly affected areas. The volume of ejecta shaped as a prism with irregular curvilinear bases, $V_{E,P,thick+thin}$, was then estimated as

$$V_{E,thick+thin} = \sum_{i=1}^{m} A_{E,thick,i} * H_{E,thick,i} + \sum_{j=1}^{n} A_{E,thin,j} * H_{E,thin,j} \qquad \text{Eq. 1}$$

where $A_{E,thick,i}$ and $H_{E,thick,i}$ are the area and the height, respectively, of a thick ejecta layer, $A_{E,thin,j}$ and $H_{E,thin,j}$ are the area and the height, respectively, of a thin ejecta layer.

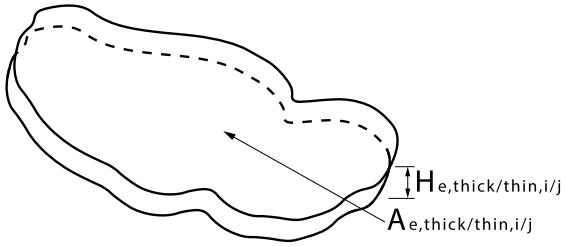

Figure 4: Sketch of ejecta shaped as a prism with irregular curvilinear bases.

Ejecta on the road were typically shaped as a series of triangular-base prisms with different dimensions (Figure 5). The rectangular shapes of ejecta on the road were first outlined on the high-resolution aerial photographs for each Canterbury earthquake. The dimensions of each ejecta rectangle were measured using the Google Earth tools. The width of a rectangle (i.e., the height of a triangle of a prism's base), $W_{E,prism,k}$, is perpendicular to the curb, while the length of a rectangle (i.e., the height of a prism), $L_{E,prism,k}$, aligns with the curb. The lower and upper estimates of the height of ejecta at the curb (i.e., the length of a prism's triangular base), $H_{E,prism,k}$, were based on the typical cross-slopes of normal crown of 2% and 4%, respectively; that is

$$H_{E,prism,k} = slope * W_{E,prism,k}. \qquad Eq.\ 2$$

The height of ejecta was capped at a typical curb height of 150 mm unless ejecta extended above the curb and onto the ground surface toward properties, in which case ejecta were estimated to be as high as 300 mm. The volume of ejecta shaped as a triangular-base prism, $V_{E,prism}$, was estimated as

$$V_{E,prism} = \frac{1}{2}\sum_{k=1}^{p} W_{E,prism,k} * H_{E,prism,k} * L_{E,prism,k}. \qquad Eq.\ 3$$

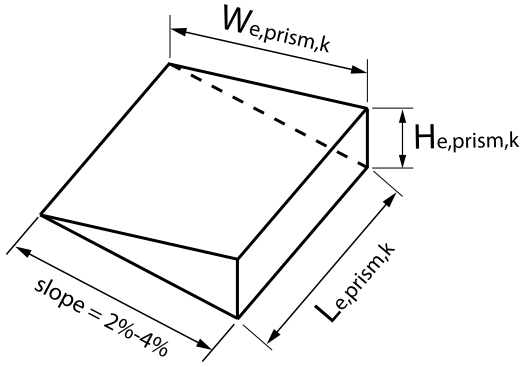

Figure 5: Sketch of ejecta on the road shaped as a prism with triangular bases.

Ejecta that occurred naturally in a form of an isolated cone (Figure 6) had its area $A_{E,cone,l}$ measured on the high-resolution aerial photograph in Google Earth and its height $H_{E,cone,l}$ estimated based on the best available physical evidence to obtain the volume, $V_{E,cone}$, as

$$V_{E,cone} = \frac{1}{3}\sum_{l=1}^{r} A_{E,cone,l} * H_{E,cone,l}. \qquad Eq.\ 4$$

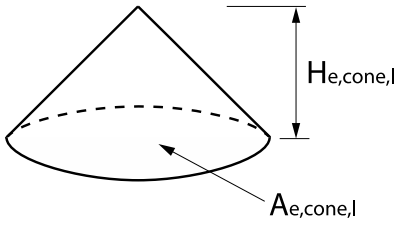

Figure 6: Sketch of ejecta occurring naturally as a cone.

When ejecta were cleaned from properties and roads into a pile, the pile consisted usually of an isolated cone or partially overlapping cones of ejecta with an assumed angle of repose of 30° (Figure 7). The radius of a cone's circular base, $R_{E,cc,s}$, was measured in Google Earth and the height of a conically shaped pile component, $H_{E,cc,s}$, was approximated as

$$H_{E,cc,s} = R_{E,cc,s} * \tan(30°). \qquad Eq.\ 5$$

The volume of piled ejecta was estimated as

$$V_{E,cc} = \frac{1}{3}\sum_{s=1}^{t} A_{E,cc,s} * H_{E,cc,s}. \qquad Eq.\ 6$$

where $A_{E,cc,s}$ is the area of a conically shaped pile component obtained by measuring in Google Earth.

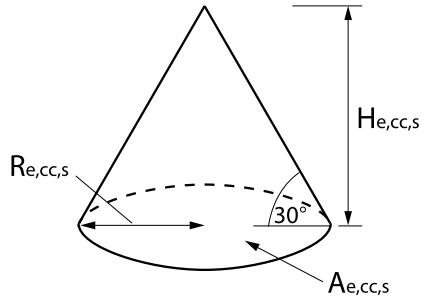

Figure 7: Sketch of a conically shaped ejecta pile that was formed as a result of cleaning efforts.

The volumes of all differently shaped ejecta present within the settlement assessment area were then added up and divided by the total settlement assessment area, A_T, to obtain the ejecta-induced settlement, $S_{E,P}$. The $S_{E,P}$ values for each site and all estimates leading to them were provided in Appendix A – Tables 9 and 10 in each site description. In addition, the photograhic-based localized ejecta-induced settlement, $S_{E,P\_localized}$, as the quotient of the total volume of ejecta, V_E, within A_T and the total coverage area of ejecta, A_E, within A_T was provided in

Appendix A – Table 14 in each site description for comparison with $S_{E,P}$ (termed S_{E,P_areal} in Appendix A – Table 14). These estimates are important in cases when ejecta do not cover A_T completely, which is when S_{E,P_areal} would be lower than $S_{E,P\_localized}$ due to areal averaging of ejecta-induced settlement.

2.2.2 LiDAR-based ejecta-induced settlement

The first step in determining the free-field ejecta-induced settlement using the LiDAR-based approach is to identify the location of a site relative to the LiDAR flight error bands and the apparent zones of higher (and lower) ground surface subsidence and account for any errors (CGD 2012c) and to estimate the vertical tectonic movement of a site for each earthquake (CGD 2012c). This information was used to populate Appendix A – Table 2 in each site description. Appendix A – Table 2 in each site description also summarizes the adjustments for each earthquake event due to the global offset, i.e., due to subtracting the post-earthquake ground surface elevations from the pre-earthquake ground surface elevations wherein both the pre-earthquake and post-earthquake LiDAR survey point elevations have an approximate median error (the accuracy of the measured elevations relative to the corresponding LINZ benchmarks).

LAS files containing LiDAR point cloud data were imported into Global Mapper to determine the ground surface elevation within the settlement assessment area for a site. After removing visible vegetation, buildings, and similar features, the remaining points were selected to compute the average ground surface (a centroid of the selected points). This was performed for each LiDAR survey, i.e., the July 2003, Sep 2010, Mar 2011, May 2011, Sep 2011, Feb 2012, and Oct 2015 surveys, to evaluate the change in the ground surface elevation due to each earthquake. For instance, the change in the ground surface elevation within the settlement assessment area due to the Sep 2010 earthquake was calculated by subtracting the average ground surface elevation of the Sep 2010 LiDAR survey points from the average ground surface elevation of the July 2003 LiDAR survey points. The earthquake-induced change in ground surface elevation can be found in Appendix A – Table 5 in each site description (termed as raw liquefaction-related ground surface subsidence using original LiDAR points). These values were then adjusted for the LiDAR flight error, vertical tectonic movement, and presence of ejecta at a site at the time of a LiDAR survey, i.e., the values listed in Appendix A – Table 2 in each site description. The obtained liquefaction-induced ground surface subsidence for each earthquake was provided in Appendix A – Table 6 in each site description.

Considering that liquefaction effects in Christchurch and its suburbs were not significant for earthquakes that occurred between Feb 2011 and June 2011, the Mar 2011 and May 2011 LiDAR surveys were used to estimate the repeat measurement error as the absolute difference between the Mar 2011 and May 2011 ground surface elevations averaged over the assessment area (Appendix A – Table 3 in each site description). The repeat measurement error was also calculated for the Feb 2012 and Oct 2015 ground surface elevations for sites without anthropogenic changes during the in-between period (Appendix A – Table 3). Averaging the surveyed elevations over an area had to have an impact on the standard deviation of the LiDAR measurement error (the accuracy of the supplied LiDAR points relative to the LINZ benchmarks) provided by Russell and van Ballegooy (2015) for individual points for each LiDAR survey. Hence, the standard deviations available for each set of pre-earthquake and post-earthquake LiDAR surveys were combined. The standard deviation obtained for each main Canterbury earthquake was multiplied by the maximum percent change in standard deviation (the ratio of the repeat measurement error and the standard

deviation for individual points, Appendix A – Table 3 in each site description). The adjusted standard deviation values are provided in Table 4 of the Appendix and rounded to the nearest 25 mm in Appendix A – Table 6 in each site description.

The estimated liquefaction-induced ground surface subsidence for each main Canterbury earthquake (Appendix A – Table 6), was compared with the coarse estimate of liquefaction-induced ground surface subsidence based on the corresponding LiDAR DEM. The latter values had to be corrected for the appropriate LiDAR flight errors (listed in Appendix A – Table 2 for each site) and the presence of ejecta at a site at the time of a LiDAR survey and were then reported in Appendix A – Table 7. The two sets of liquefaction-induced settlement estimates were presented on a bar graph (after Appendix A – Table 7 in each site description). The LiDAR DEM-based values of liquefaction-induced settlement were not used in calculations of the ejecta-induced settlement. They served primarily as a sanity check of the values in Appendix A – Table 6.

Finally, the volumetric settlement due to sedimentation and post-liquefaction reconsolidation, S_{V1D}, was subtracted from the total liquefaction-induced settlement, S_T, given in Appendix A – Table 6 in each site description, to obtain the free-field liquefaction ejecta-induced settlement, $S_{E,L}$. The shear-induced ground settlement was neglected because the select case histories originated from the free-field sites (i.e., sites without heavy buildings). The S_{V1D} was computed in *Cliq v.3.0.3*.2 using the Zhang et al. (2002) procedure which used the factor of safety against liquefaction, FS_L, from the Boulanger and Idriss (2016) procedure. The input parameters were the median PGA by Bradley and Hughes (2012), probability of liquefaction, P_L, of 50% (the actual site response is compared to the median estimate to remove bias), I_c cutoff value of 2.6 as a threshold between liquefiable and non-liquefiable soil (Lees et al. 2015), C_{FC} of 0.13 developed for Christchurch soil by Maurer et al. (2019), and the groundwater table depth at the time of each earthquake (CGD 2014). The 13 June 2011 earthquake was modeled as a M_w 6.2 earthquake to account for the excess pore water pressure that resulted from the first M_w 5.3 June 2011 earthquake and did not dissipate fully at the time of the second M_w 6.0 June 2011 earthquake that occurred 80 min later (van Ballegooy et al. 2014). By the same reasoning, the Dec 2011 earthquake was modeled as a M_w 6.1 earthquake.

The CPTs used to evaluate S_{V1D} for each settlement assessment area of a site are listed in Table 12 in the Appendix A, while the S_{V1D} values for each CPT are summarized in Appendix A – Table 13 in each site description. Appendix A – Table 13 also contains the LSN, LPI, and depth to the first layer with $FS_L<1$ that is at least 200-mm thick (crust thickness). The average S_{V1D} for each settlement assessment area was estimated for each earthquake and was reported in Appendix A – Table 8 for each site along with the moment magnitude, median PGA, and groundwater table depth for each earthquake. Because the Zhang et al. (2002) procedure does not account for uncertainty in the volumetric settlement estimates, the sensitivity of volumetric settlement to PGA, C_{FC}, and P_L for each earthquake event was derived for two sites (VsVp 57203 Shirley Intermediate School and CPT 5586 – Vivian St). Taking the 50th percentile as the baseline case, the minimum and maximum values correspoding to the difference between the 25th percentile and the 50th percentile and the 75th percentile and the 50th percentile were estimated. The arithmetic mean of the range of the minimum and maximum difference was evaluated for each assessment area of the two sites. The maximum arithmetic mean for each earthquake event was rounded to the nearest five mm and was used as the uncertainty value. Accordingly, the volumetric settlement uncertainties of ± 20, ± 50, ± 25, and ± 50 mm for the Sep 2010, Feb 2011, Jun 2011, and Dec 2011 earthquakes, respectively, were used for all sites in this study. Finally, $S_{E,L}$ as the difference between S_T and S_{V1D} was also added to Appendix A – Table 8 in each site description.

2.2.3 Best final estimates of ejecta-induced settlement

Once the free-field liquefaction ejecta-induced settlement was estimated using both the photographic evidence-based method and LiDAR-based method, the best final estimate of the ejecta-induced settlement, $S_{E,final}$, was provided in Appendix A – Table 11 in each site description as the weighted average of the two estimates. This was done for each settlement assessment area and each earthquake. The weighting coefficients were based typically on the LiDAR measurement errors, misestimates of liquefaction severity using the liquefaction triggering procedures as per Maurer et al. (2014), and completeness of visual evidence. Table 3 summarizes the best final estimates of the ejecta-induced free-field settlement for the 61 sites.

Table 3: Best final estimates of ejecta-induced free-field settlement for each site.

Site ID	SPC	Sep 2010		Feb 2011		Jun 2011		Dec 2011		Ejecta-Induced Free-Field Settlement [mm]			
		LSN	LPI	LSN	LPI	LSN	LPI	LSN	LPI	Sep 2010	Feb 2011	Jun 2011	Dec 2011
VsVp 57203	1	1	0	13	5	2	0	5	1	0	125 ±25	50 ±15	<5
VsVp 57190	4	9	2	15	7	1	0	0	0	<5	30 ±10	0	0
VsVp 57188	1	0	0	2	1	0	0	1	0	0	0	0	0
VsVp 38175	4	20	8	20	9	1	0	1	0	<5	0	0	0
VsVp 57142	1	15	4	13	3	1	0	1	0	0	0	0	0
CPT 5586	1	1	0	11	4	4	1	13	4	0	80 ±30	40 ±30	<5
VsVp 57195	1	1	0	10	4	3	0	8	2	0	70 ±70	<5	0
CPT 27709	1	2	0	12	4	4	0	13	5	0	90 ±25	20 ±10	5 ±5
CPT 49582	1	7	1	16	7	4	0	11	3	0	10 ±5	0	<5
CPT 61991	1	1	0	16	8	1	0	13	5	0	25 ±5	10 ±5	5±5
VsVp 57193	1	0	0	10	5	1	0	1	0	0	<5	0	0
VsVp 57062	1	1	0	17	7	11	2	8	2	0	60 ±45	30 ±65	0
CPT 3937	1	2	0	9	6	2	0	9	4	0	95 ±35	20 ±5	10 ±5
CPT 90678	1	4	0	22	11	6	2	17	8	0	120 ±30	85 ±25	65 ±15
CPT 44959	4	4	0	9	3	6	1	7	1	5 ±5	40 ±10	15 ±20	<5
CPT 4674	1	2	0	22	8	14	3	17	5	0	90 ±30	20 ±20	5 ±5
CPT 15498	1	1	0	14	7	3	0	9	2	0	50 ±10	10 ±5	0
CPT 29778	1	0	0	5	1	0	0	13	3	0	15 ±20	<5	<5

Site ID	SPC	Sep 2010		Feb 2011		Jun 2011		Dec 2011		Ejecta-Induced Free-Field Settlement [mm]			
		LSN	LPI	LSN	LPI	LSN	LPI	LSN	LPI	Sep 2010	Feb 2011	Jun 2011	Dec 2011
CPT 5261	1	3	0	20	11	12	3	14	5	0	130 ±35	50 ±15	25 ±5
VsVp 57320	1	1	0	--	--	--	--	--	--	5 ±5	--	--	--
VsVp 57326	4	9*	2*	--	--	--	--	--	--	0	--	--	--
CPT 44439	1	7	1	34	17	15	3	16	3	25 ±5	50 ±10	40 ±10	10 ±5
VsVp 57200	4	6	1	--	--	--	--	--	--	0	--	--	--
VsVp 57191	3	38	17	41	25	16	2	12	1	0	0	0	0
VsVp 57182	2	25*	10*	25*	19*	9*	2*	1*	0*	0	10 ±5	0	0
VsVp 57186	1	19	5	41	28	33	16	14	4	0	25 ±10	20 ±5	<5
VsVp 57187	1	12	1	34	19	35	14	29	12	0	20 ±10	10 ±5	5±5
VsVp 57192	4	0	0	1	1	0	0	1	0	0	50 ±10	30 ±10	5 ±5
VsVp 38172	3	21	8	31	18	12	2	4	0	0	15 ±5	<5	0
CPT 6551	1	2	0	17	12	8	2	14	5	0	25 ±25	25 ±20	0
CPT 62594	1	3	1	15	8	4	1	16	7	0	35 ±10	10 ±5	5±5
CPT 54376	1	7	1	19	9	7	1	11	3	0	75 ±25	25 ±5	0
CPT 33732	1	8	3	13	9	2	0	1	0	0	65 ±20	0	0
CPT 17908	2	2	0	15	8	8	2	3	0	0	40 ±25	20 ±20	10 ±5
CPT 14070	1	5	1	21	14	12	3	20	9	0	155 ±40	105 ±10	120 ±20
CPT 44440	1	16	5	31	25	20	10	13	4	0	90 ±20	30 ±5	0
CPT 25514	1	2	0	10	6	5	1	3	0	0	5 ±5	5 ±5	0
CPT 5687	1	10	2	26	17	12	5	6	2	0	35 ±10	15 ±5	0
CPT 27040	1	2	0	18	9	4	1	32	9	0	95 ±30	75 ±55	15 ±5
CPT 2168	1	2	0	14	6	5	1	23	7	0	55 ±30	35 ±35	5 ±5
CPT 17200	1	1	0	15	7	3	0	6	1	<5	90 ±30	25 ±20	0
VsVp 57165	2	12	3	22	12	3	0	2	0	0	0	0	0
VsVp 57181	2	13	4	22	12	5	0	8	1	40 ±10	25 ±10	15 ±5	<5

Site ID	SPC	Sep 2010		Feb 2011		Jun 2011		Dec 2011		Ejecta-Induced Free-Field Settlement [mm]			
		LSN	LPI	LSN	LPI	LSN	LPI	LSN	LPI	Sep 2010	Feb 2011	Jun 2011	Dec 2011
VsVp 57201	3	22	8	28	19	5	0	0	0	0	10 ±5	0	0
VsVp 57180	2	12	3	23	12	8	1	8	1	0	5 ±5	<5	0
CPT 29740	1	5	1	24	12	10	2	21	8	0	80 ±45	70 ±40	65 ±20
CPT 25981	1	2	0	17	7	2	0	13	4	0	60 ±15	25 ±10	30 ±5
CPT 56468	1	3	0	18	7	2	0	9	1	0	25 ±10	25 ±20	10 ±5
CPT 59661	1	7	1	33	17	12	1	9	1	40 ±10	75 ±10	25 ±5	15 ±5
VsVp 57185	1	14	4	41	33	29	15	12	3	0	0	0	0
CPT 62761	1	22	5	48	43	38	24	18	3	0	35 ±10	30 ±5	0
CPT 17262	1	4	0	26	17	11	2	3	0	0	60 ±15	10 ±5	0
VsVp 38176	3	33	20	30	25	12	2	4	0	0	0	0	0
VsVp 57189	2	17*	5*	22*	8*	4*	0*	7*	1*	0	0	0	0
CPT 28986	1	1.0	0	5	2	1.0	0	0	0	0	0	0	0
VsVp 38171	3	16	8	19	14	10	3	2	0	0	0	0	0
CPT 45795	1	2	0	7	4	3	1	2	0	0	0	0	0
CPT 54736	1	1	0	6	2	1	0	5	1	0	0	0	0
CPT 88252	3	4	1	12	3	1	0	3	0	0	0	0	0
CPT 128494	1	0	0	2	2	0	0	2	1	0	0	0	0
VsVp 57155	3	20	7	18	6	1	0	2	0	0	0	0	0

Notes: SPC = Soil Profile Categories, which can be defined as (1) thick, clean sand, (2) partially stratified, (3) highly stratified silty soil, and (4) gravel-dominating soil profile; The LSN and LPI were averaged typically over a 50-m buffer; * indicates that LSN and LPI were calculated to a cone penetration depth that is shallower than 20 m.

3. DETAILED EVALUATION OF SELECT CASE HISTORIES

3.1 Shirley Intermediate School

The Shirley Intermediate School site is situated in the NE geologic quadrant of Christchurch (172.661995°, -43.510408°). It is a level, open-field site that did not undergo lateral spreading for any of the four main Canterbury earthquakes. The nearest free-face feature is a creek that is approximately 55 m to the SE from the center of the site. The road passes through the eastern portion of the site's 50-m buffer and covers approximately 15% of its area. The site is covered in

grass and its primary use is for sports activities. Ten percent of the site's 50-m buffer is occupied by school buildings, which were constructed in the period between Apr 2011 and Jun 2011. Some minor earthwork was performed at the same southern portion of the site between Oct 2009 and Feb 2011. This information is based on the historical satellite images available for the period from Apr 2004 to present. Trees, bushes, and plants other than grass (all termed vegetation) cover 10% of the 20-m buffer and 20% of the 50-m buffer. All these features and anthropogenic changes were considered when selecting the settlement assessment area as they could affect the LiDAR survey measurements. Therefore, the area selected for the ejecta-induced settlement analysis excludes vegetation, buildings, and significant anthropogenic changes (Figure 8). This area also has good spatial distribution of ejecta (Figure 9). Detailed site description for the 10-, 20-, and 50-m buffers is provided in Table 4 (an equivalent of Table 1 in Appendix A for this site).

The aerial photographs in Figure 9 were used to determine the occurrence of ejecta at the site and to measure the area of ejecta coverage within the assessment area (the red outline). The absence of ejecta is evident for the Sep 2010 earthquake. For the Feb 2011, ejecta occurred in an anastomosing pattern rather than as individual conically shaped soil boils. Ejecta were distributed spatially across the site. Different shades of gray of the ejecta were interpreted as different ejecta thicknesses. The light gray ejecta outlined in yellow were classified as thin ejecta, while the dark gray ejecta outlined in pink were classified as thick ejecta. The total areas of the outlined thick ejecta layers and the outlined thin ejecta layers ($A_{E,thick}$ and $A_{E,thin}$, respectively) were measured in Google Earth™. The $A_{E,thick}$ and $A_{E,thin}$ values for the 20-m buffer are summarized in Table 5. In the absence of ground photographs, the height range for the thick and thin ejecta layers ($H_{E,thick}$ and $H_{E,thin}$, respectively), was estimated based on the typical height of similar-looking ejecta for the neighboring area and statements made by locals. Finally, the volume of ejecta was estimated using Eq. 1 and was divided by the total assessment area, A_T, to obtain the ejecta-induced free-field settlement, $S_{E,P}$ (Table 6). The areal $S_{E,P}$ was then compared with the localized ejecta-induced settlement, $S_{E,P\_localized}$ (Table 7), which was obtained by dividing the total volume of ejecta within A_T by the total coverage area of ejecta within A_T. Figure 9 also shows the presence of ejecta for the June 2011 earthquake. However, ejecta appeared to be cleaned partially from the site. To account for this uncertainty, the height of ejecta was provided as a wider range, while assuming that ejecta covered the portion of the site in light brown color. The area for the June 2011 earthquake reported in Table 5 corresponds to the area outlined in orange and within the 20-m buffer. Also, cars and construction equipment obscured a portion of the assessment area in the June 2011 aerial photograph, resulting in that portion of the site being excluded from the analysis. For the Dec 2011 earthquake, only minor ejecta (outlined in yellow in Figure 9) were present.

To estimate the LiDAR-based ejecta-induced settlement, the change in ground surface elevation within the asessment area was determined for individual LiDAR points, such as those shown in Figure 10, for each earthquake (Table 8). These values were then adjusted for the LiDAR flight error, global offset, and tectonic movement (Table 9). The site is in the apparent zone of the higher ground surface subsidence for the Sep 2011 earthquake and the apparent zone of lower ground surface subsidence for the Feb 2011 earthquake (Figure 11). To account for this LiDAR flight error, 100 mm were subtracted from the ground surface elevation change in Table 8 for the Sep 2011 earthquake and 100 mm were added to the ground surface elevation change in Table 8 for the Feb 2011. The final estimates of liquefaction-induced ground surface subsidence provided in Table 10 were compared with the coarse estimates of the ground surface subisdence using the LiDAR DEMs (Figure 12). No major discrepancies between the two sets of estimates were observed. The average S_{V1D} was then calculated and subtracted from the values in Table 10 to

obtain $S_{E,L}$ (Table 11). The PGA ranged from 0.19 g for the Sep 2011 earthquake to 0.38 g for the Feb 2011 earthquake. The depth to the groundwater table was in the range from 2.0 m below ground surface (BGS) for the Dec 2011 earthquake to 2.5 m BGS for the Feb 2011 earthquake. All CPTs shown in Figure 13 were used to calculate the average S_{V1D} for the 50-m buffer (four of them were outside the 50-m buffer, CPT 4066 was 90 m away from the center of the site), whereas only CPTs 4065 and 56891 were used to calculate the average S_{V1D} for the 10-m and 20-m buffers. The S_{V1D} values for individual CPTs for each earthquake event are provided in Table 12.

The $S_{E,L}$ values in Table 11 were used in combination with the $S_{E,P}$ values in Table 6 to provide the best final estimate of ejecta-induced free-field settlement, $S_{E,final}$ (Table 13). The $S_{E,final}$ represents the weighted average of $S_{E,L}$ and $S_{E,P}$ with respective weight coefficients of 1/3 and 2/3 for the Feb 2011 and June 2011 earthquakes and the respective weight coeffecients of 0 and 1 for the Sep 2010 and Dec 2011 earthquakes. The lower weight coefficient for the Feb 2011 and June 2011 earthquakes was assigned to $S_{E,L}$ because the Shirley Intermediate School site was in the apparent zone of higher/lower ground surface movements for the Sep 2010/Feb 2011 earthquake due to the LiDAR flight error and had slight to moderate underestimates of liquefaction manifestation at the ground surface than was observed (Maurer et al. 2014). $S_{E,L}$ was not given any weight for the Sep 2010 and Dec 2011 earthquakes due to the evident absence of ejecta for the Sep 2010 earthquake and due to negligible ejecta and negative $S_{E,L}$ values for the Dec 2011 earthquake. The best estimate of the ejecta-induced free-field ground settlement at the Shirley Intermediate School site for the Sep 2010, Feb 2011, June 2011 is 0 mm, 125 ± 25 mm, 50 ± 15 mm, and <5 mm, respectively, considering that the 10-m buffer is the most representative buffer in terms of spatial distribution of ejecta over the site.

The soil profile at the Shirley intermediate site can be described using the available borehole log and CPTs. The site can be classified as a thick, clean sand site because a borehole log at the center of the site indicates a 5-m thick layer of fine to medium sand, SP, in the upper 10 m (from the 3.4- to 8.2-m depth) and below the average groundwater table depth of 1.6 m BGS. This marine/estuarine SP layer of the Christchurch formation has an average q_t of 9 MPa. The top 3.4 m of the soil profile consist of the 0.4-m thick organic silty, OL, topsoil ($q_{t,avg}$ = 4 MPa) and underlying interchangeable layers of alluvial non-plastic to low plasticity silt, ML, and alluvial silty sand, SM, of the Springston formation ($q_{t,avg}$ = 4 MPa). Below the 8.2-m depth, sandy subrounded marine/estuarine gravel, GW, with $q_{t,avg}$ = 15 MPa extends to a depth of 11.1 m and overlies fine to coarse marine/estuarine sand, SP, to a depth of 20 m. The provided q_t values corrected for thin-layer effects using the de Greef and Lengkeek (2018) procedure are based on CPTs 4065 and 56891. Two additional CPTs from outside the 50-m buffer show the presence of gravelly layers at depths shallower than 8 m close to the rim of the 50-m buffer.

Finally, all available CPTs were used to estimate the average crust thickness. The depth to the first $FS_L < 1$ layer that is at least 200-mm thick was 3.1 m and 4.0 m for the Feb 2011 and Dec 2011, respectively. For the Sep 2010 and June 2011 earthquakes, the 200-mm thick layer with $FS_L < 1$ did not exist (Table 12). The average crust thickness was also defined as the depth to the first $I_c < 2.6$ layer that is at least 200-mm thick and below the groundwater table. These values are not provided in the Appendix, but the electronic supplement only. They were estimated as 2.7, 2.7, 2.6, and 2.5 m BGS for the Sep 2010, Feb 2011, June 2011, and Dec 2011, respectively. Also, the average LPI = 0, 5, 0, and 1 and LSN = 1, 13, 2, and 5 for the Sep 2010, Feb 2011, Jun 2011, and Dec 2011 earthquakes, respectively. Considering the observations of liquefaction ejecta (Figure 9), the severity of liquefaction manifestation at the ground surface was higher than estimated by LPI or LSN for the Feb 2011 and June 2011 earthquakes and was correctly estimated for the Sep 2010 and Dec 2011 earthquakes.

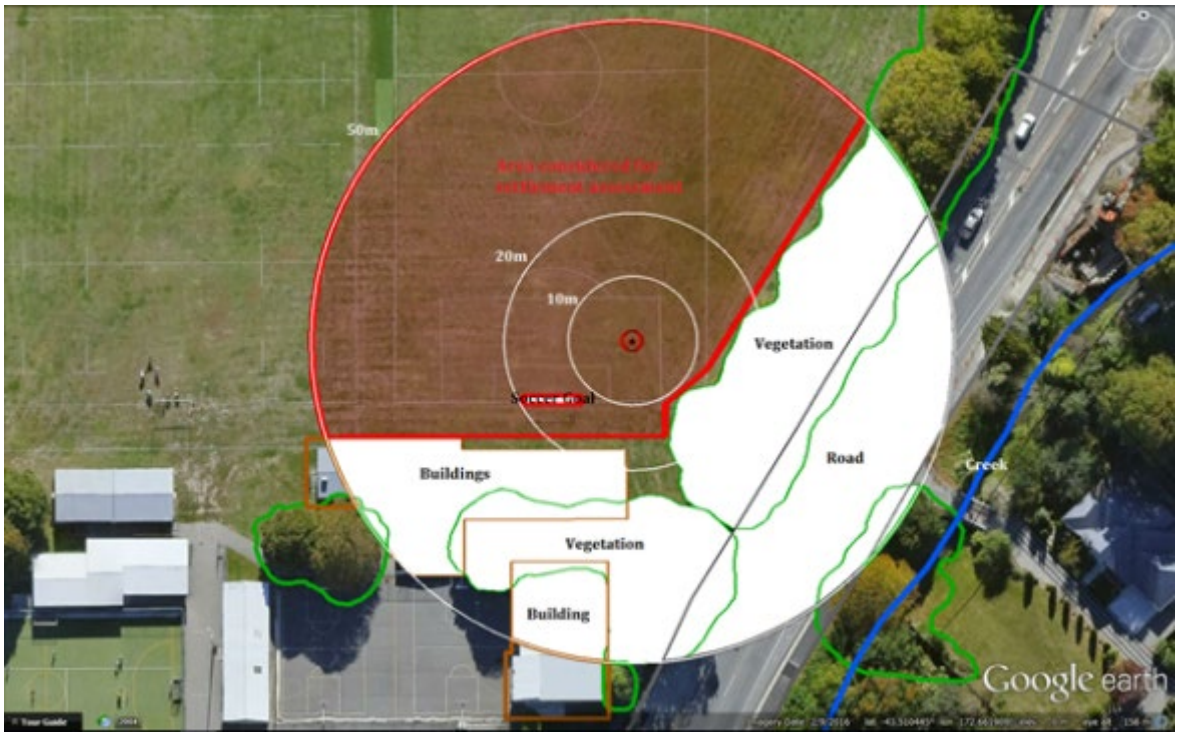

Figure 8: The Shirley Intermediate School site plan with the area analyzed for ejecta-induced settlement.

Figure 9: Aerial photographs acquired for Shirley Intermediate School in Sep 2010, Feb 2011, June 2011, and Dec 2011 *(CGD 2012a)* with ejecta outlines for the 10-, 20-, and 50-m buffers.

Table 4: Site Description for Shirley Intermediate School (V_sV_p 57203).

Attribute	Yes/No			Description/Date	Symbol in Figure 1
	10-m Buffer	20-m Buffer	50-m Buffer		
Near a body of surface water or other free face features?	No	No	No	The centre of the site is 55 meters to the NW of the creek. The direction of the free face is roughly NE-SW, while its height is approximately 2.5 m.	Blue Outline
Lateral spreading observed during the CES?	No	No	No	Ground cracks indicating lateral spreading were not observed by the mapping team.	NA
Nearby buildings or structures?	No	No	Yes	Several school buildings are approximately 20 m away from the centre of the site, localized in the SW portion of the 50-m buffer and covering 10% of its area.	White Fill + Brown Outline
Sloping land?	No	No	No	Flat land, sports ground.	NA
Step changes in the ground surface?	No	No	No	NA	NA
Retaining walls?	No	No	No	NA	NA
Vegetation?	No	Yes	Yes	Trees cover 10% of the 20-m buffer and 20% of the 50-m buffer. They are in the E portion of the 20-m buffer and the NE, SE, and SW quadrants of the 50-m buffer.	White Fill + Green Outline
Anthropogenic changes to the site between the LiDAR surveys?	No	Yes	Yes	Three school buildings were added between Apr 2011 and June 2011 earthquake. They are in the SW quadrant of the 50-m buffer and cover 7% of the area. They also spread to the southern part of the 20-m buffer, affecting 1% of the area. Minor earthwork in the southern portion of the 50-m buffer was performed sometime between Oct 2009 and Feb 2011.	White Fill + Brown Outline
Other important factors?	No	No	Yes	Road occupies 15% of the 50-m buffer and stretches throughout the NE and SE quadrants.	Road: White Fill + Gray Outline

Note: Buffer is the area within a circle of a specified radius (i.e., 10 m, 20 m, or 50 m) with VsVp investigations done at its center (172.661995°, -43.510408°).

Table 5: Coverage area and height of ejecta estimates for 20-m buffer using photographs.

Earthquake Event	$A_{E,thick}$ [m^2]	$H_{E,thick}$ [mm]	$A_{E,thin}$ [m^2]	$H_{E,thin}$ [mm]	A_T [m^2]
Sep 2010	0	0	0	0	1003
Feb 2011	594	150-250	171	50-100	1003
Jun 2011	439	30-100	0	0	938*
Dec 2011	0	0	18	10-20	1003

Notes: A_T = Total assessment area of a radial area being considered; * indicates that A_T is lower due to the presence of objects (e.g., vehicles and construction equipment/material) at portions of the site at the time the aerial photograph was acquired.

Table 6: Ejecta-induced settlement estimates based on photographs.

Earthquake Event	10-m buffer		20-m buffer		50-m buffer	
	$S_{E,P,lower}$ (mm)	$S_{E,P,upper}$ (mm)	$S_{E,P,lower}$ (mm)	$S_{E,P,upper}$ (mm)	$S_{E,P,lower}$ (mm)	$S_{E,P,upper}$ (mm)
Sep 2010	0	0	0	0	0	0
Feb 2011	75	126	97	165	56	95
Jun 2011	11	35	14	47	9	30
Dec 2011	≈0	≈0	≈0	≈0	≈0	≈0

Note: $S_{E,P,lower}$ and $S_{E,P,upper}$ correspond to lower and upper estimates of $S_{E,P}$, respectively.

Table 7: Comparison of photographic-based areal and localized ejecta-induced settlement.

Earthquake Event	10-m buffer		20-m buffer		50-m buffer	
	S_{E,P_areal} (mm)	$S_{E,P\_localized}$ (mm)	S_{E,P_areal} (mm)	$S_{E,P\_localized}$ (mm)	S_{E,P_areal} (mm)	$S_{E,P\_localized}$ (mm)
Sep 2010	0	0	0	0	0	0
Feb 2011	100±25	175±45	130±35	175±45	75±20	175±45
Jun 2011	25±10	65±35	30±15	65±35	20±10	65±35
Dec 2011	<5	15±5	<5	15±5	<5	15±5

Notes: $S_{E,P,lower}$ and $S_{E,P,upper}$ correspond to lower and upper estimates of $S_{E,P}$, respectively; The estimates are rounded to the nearest 5 mm.

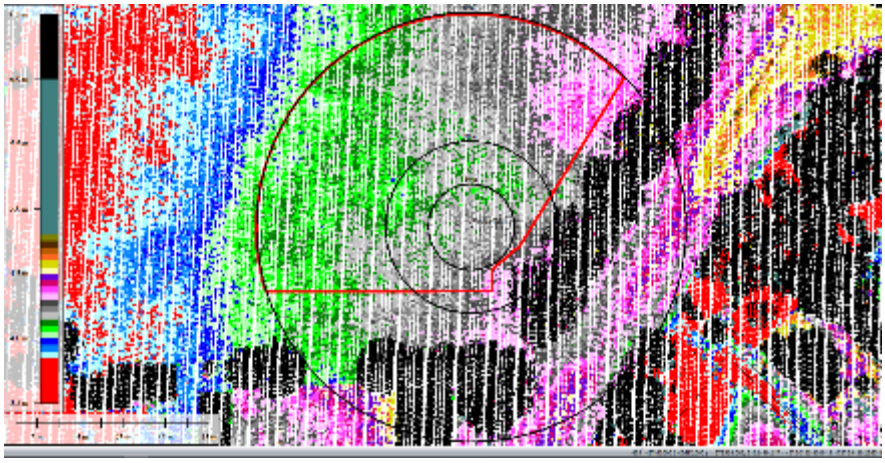

Figure 10: LiDAR survey points used to compute the average elevation in Global Mapper within the assessment area (outlined in red) for Mar 2011.

Table 8: Raw liquefaction-related ground surface subsidence using original LiDAR points.

	Average Ground Surface Subsidence (mm)		
Earthquake Event(s)	10-m Buffer	20-m Buffer	50-m Buffer
Sep 2010	134	138	124
Feb 2011	214	213	148
Jun 2011	114	98	75
Dec 2011	7	12	15
CES	469	461	362

Table 9: LiDAR flight error adjustments, global adjustments for the difference between average LiDAR point elevations and benchmark survey elevations, and vertical tectonic movement adjustments.

	Adjustments (mm)		
Earthquake Event(s)	LiDAR Flight Error	Global Offset	Tectonic Vertical Movement
Sep 2010	-100	-3	0
Feb 2011	100	16	-85
Jun 2011	0	38	-40
Dec 2011	0	-65	0
CES	0	-14	-125
Any LiDAR survey affected by ejecta?			No

Note: The negative sign indicates the subtraction from the ground surface subsidence, while the positive sign indicates the addition to the ground surface subsidence.

Table 10: Corrected liquefaction-related ground surface subsidence using original LiDAR points and the adjustments in Table 9.

	Average Calculated Ground Surface Subsidence (mm)		
Earthquake Event(s)	10-m Buffer	20-m Buffer	50-m Buffer
Sep 2010	31±75	35±75	21±75
Feb 2011	245±25	244±25	179±25
Jun 2011	112±25	96±25	73±25
Dec 2011	-58±50	-53±50	-50±50
CES	330±75	322±75	223±75

Notes: Plus/minus values are rounded to the nearest 25 mm; Positive overall values indicate ground surface subsidence, while negative overall values idicate ground surface uplift.

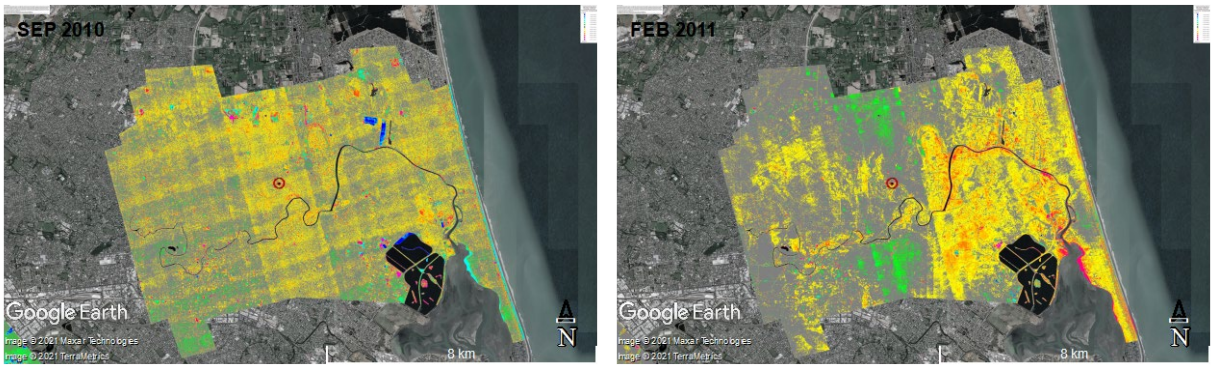

Figure 11: Vertical Ground Movements (adjusted for the tectonic component) for the Sep 2010 and Feb 2011 earthquakes *(CGD 2015a)* – the site is in the apparent zone of overestimated ground surface subsidence for the Sep 2010 earthquake and the apparent zone of underestimated ground surface subsidence for the Feb 2011 earthquake.

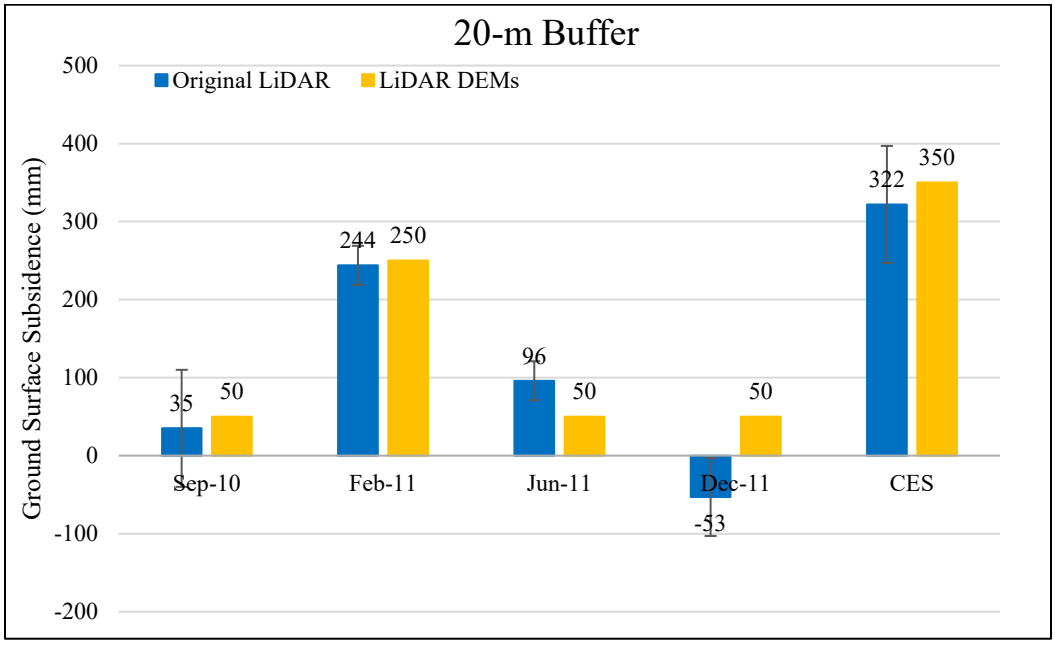

Figure 12: Comparison between the ground surface subsidence determined using the individual LiDAR elevation points and the ground surface subsidence estimated using the LiDAR DEMs.

Table 11: Ejecta-induced settlement for the top 20 m of the soil profile within the 20-m buffer for the 50th %ile PGA, P_L=50%, and C_{FC}=0.13 using BI-2016, ZRB-2002, and I_C cutoff of 2.6.

Earthquake Event	M_W	PGA (g)	Depth to Groundwater (m)	S_T (mm)	S_{V1D} (mm)	$S_{E,L}$ (mm)
Sep 2010	7.1	0.19	2.5	35±75	7±20	28±78
Feb 2011	6.2	0.38	2.5	244±25	71±50	173±56
Jun 2011	6.2	0.22	2.2	96±25	10±25	86±35
Dec 2011	6.1	0.26	2.0	-53±50	25±50	-78±71

Notes: S_T = Total settlement (Table 10); S_{V1D} = Average vertical settlement due to volumetric compression using the Boulanger and Idriss (2016) (BI-2016) and Zhang et al. (2002) (ZRB-2002) procedures and the de Greef and Lengkeek (2018) thin-layer correction procedure; $S_{E,L}$ = Ejecta-induced settlement as the difference between the LiDAR-based S_T and S_{V1D}.

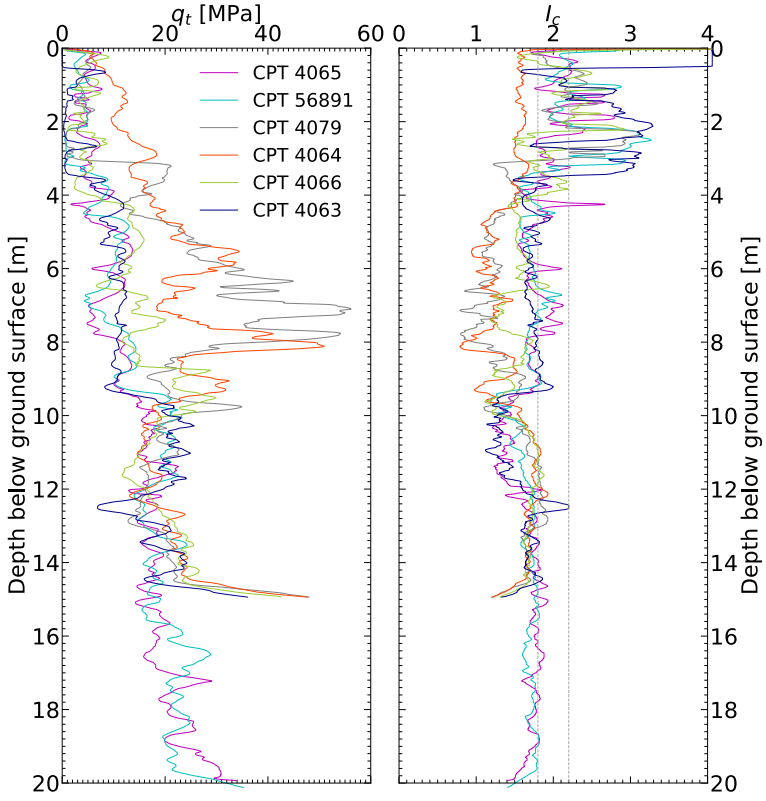

Figure 13: CPT traces for Shirley Intermediate School.

Table 12: CPT-based results for Shirley Intermediate School.

EQ Event	Parameter	CPT ID 4065	56891	4079	4064	4066	4063
Sep 2010	S_{V1D} (mm)	7	7	1	0	4	1
	LSN	1	1	0	0	1	0
	LPI	0	0	0	0	0	0
	LPI_{ish}	0	0	0	0	0	0
	$D_{FS<1}$ (m)	undet.	undet.	undet.	undet.	undet.	undet.
Feb 2011	S_{V1D} (mm)	71	70	7	0	43	36
	LSN	13	13	2	0	11	7
	LPI	5	5	1	0	4	1
	LPI_{ish}	3	4	1	0	3	1
	$D_{FS<1}$ (m)	3.20	3.18	undet.	undet.	2.72	3.45
June 2011	S_{V1D} (mm)	9	10	1	0	7	1
	LSN	2	2	1	0	2	0
	LPI	0	0	0	0	0	0
	LPI_{ish}	0	0	0	0	0	0
	$D_{FS<1}$ (m)	undet.	undet.	undet.	undet.	undet.	undet.
Dec 2011	S_{V1D} (mm)	22	28	4	0	20	6
	LSN	4	6	1	0	6	1
	LPI	0	1	0	0	1	0
	LPI_{ish}	0	1	0	0	1	0
	$D_{FS<1}$ (m)	4.27	6.70	undet.	undet.	3.45	undet.

Notes: $D_{FS<1}$ = Depth to the first liquefiable layer (FS_L<1) that is at least 200-mm thick, as determined by the Boulanger and Idriss (2016) liquefaction-triggering procedure (P_L=50%, C_{FC}=0.13, and $I_{c,cutoff}$ =2.6), and exported from Cliq v.3.0.3.2; undet. = the specified soil layer was not detected.

Table 13: Best final estimates of ejecta-induced settlement for Shirley Intermediate School.

Earthquake Event	10-m radius			20-m radius			50-m radius		
	$S_{E,L}$ (mm)	$S_{E,P}$ (mm)	$S_{E,final}$ (mm)	$S_{E,L}$ (mm)	$S_{E,P}$ (mm)	$S_{E,final}$ (mm)	$S_{E,L}$ (mm)	$S_{E,P}$ (mm)	$S_{E,final}$ (mm)
Sep 2010	24±78	0	0	28±78	0	0	18±78	0	0
Feb 2011	174±56	101±25	125±25	173±56	131±34	145±30	141±56	76±19	100±25
Jun 2011	102±35	23±12	50±15	86±35	31±17	50±15	68±35	20±11	40±15
Dec 2011	-83±71	≈0	<5	-78±71	≈0	<5	-63±71	≈0	<5

Notes: $S_{E,L}$ = Ejecta-induced settlement based on LiDAR data and reported in Table 11; $S_{E,P}$ = Median ejecta-induced settlement for the range of values in Table 6; $S_{E,final}$ = Best final estimate of ejecta-induced settlement rounded to the nearest 5 mm; Final plus/minus values are also rounded to the nearest 5 mm.

3.2 Tonks St

The Tonks St site (172.724500°, -43.493746°) is in the NE quadrant of Christchurch, approximately 200 m to the west from the Pegasus Bay. It is in the residential area that has approximately 30% of its 10-m, 20-m, and 50-m buffer covered with residential buildings. Approximately 15% of 20-m and 50-m buffers is occupied by a paved (impervious) road that passes predominantly through their eastern portions. Vegetation covers 30, 20, and 30% of the 10-m, 20-m, and 50-m buffers, respectively. No lateral spreading was observed for any earthquake event. The site is mostly level apart from the properties in the western portion of the 50-m buffer that typically have sloped driveways as they are approximately 0.5 m above the elevation of the road. The front lawns at these properties are, therefore, retained by 0.5-m tall walls. No specific area was outlined for settlement assessment at this site because ejecta were absent for all earthquake events as evident from the high-resolution aerial photographs (Figure 14). The lack of inspection reports for the properties within the 50-m buffer was an additional piece of evidence that ejecta did not occur at the site. Thus, it was not necessary to consider the LiDAR surveys to conclude that the ejecta-induced settlement at the Tonks St site for the Sep 2010, Feb 2011, June 2011, and Dec 2011 earthquake is 0 mm, 0 mm, 0 mm, and 0 mm, respectively (Table 14).

The groundwater table at the Tonks St site is at a 2.5-m depth BGS. The soil profile at the site consists primarily of fine to medium sand, SP, of marine/estuarine origin (the Christchurch formation) to a depth of 20 m, whose average q_t is 17 MPa. Thus, the soil profile at the Tonks St site belongs to the thick, clean sand category. Figure 15 illustrates the q_t and I_c traces of three CPTs available within the 50-m buffer (CPTs 128494, 128495, and 128496), while Table 15 summarizes the average volumetric settlements for each buffer along with the PGA and earthquake-specific groundwater depths. The PGA at the Tonks St site varied from 0.19 g for the Sep 2010 earthquake to 0.56 g for the Feb 2011 earthquake, while the groundwater level was at a depth range from 2.3 m BGS for the Dec 2011 earthquake to 3.3 m BGS for the Sep 2010 and Feb 2011 earthquakes.

The average crust thickness as defined by the depth to the first $FS_L < 1$ layer that is at least 200-mm thick was 8.5 m for the Feb 2011 earthquake (Table 16). The 200-mm thick layer with $FS_L < 1$ was not detected for the Sep 2010 and Jun 2011 earthquakes. For the Dec 2011 earthquake, the specified layer was detected at a depth of about 8.6-m for two CPTs and was undetected for one CPT. The average crust thickness defined as the depth to the first $I_c < 2.6$ layer below the groundwater table that is at least 200-mm thick was 3.3, 3.3, 2.5, and 2.3 m BGS for the Sep 2010, Feb 2011, June 2011, and Dec 2011 earthquakes, respectively. For the Sep 2010, Feb 2011, Jun 2011, and Dec 2011 earthquake, LPI = 0, 2, 0, and 1, respectively, and LSN = 0, 2, 0, and 2, respectively (Table 16). Therefore, the severity of liquefaction manifestation at the ground surface of the Tonks St site was captured well by state-of-the-practice liquefaction triggering procedures for all earthquake events.

Figure 14:Aerial photographs for the Tonks St site acquired in Sep 2010, Feb 2011, June 2011, and Dec 2011 *(CGD 2012a)*.

Table 14: Best final estimates of ejecta-induced settlement for Tonks St.

EQ Event	10-m buffer			20-m buffer			50-m buffer		
	$S_{E,L}$ (mm)	$S_{E,P}$ (mm)	$S_{E,final}$ (mm)	$S_{E,L}$ (mm)	$S_{E,P}$ (mm)	$S_{E,final}$ (mm)	$S_{E,L}$ (mm)	$S_{E,P}$ (mm)	$S_{E,final}$ (mm)
Sep-10	--	0	0	--	0	0	--	0	0
Feb-11	--	0	0	--	0	0	--	0	0
Jun-11	--	0	0	--	0	0	--	0	0
Dec-11	--	0	0	--	0	0	--	0	0

Notes: $S_{E,L}$ = LiDAR-based ejecta-induced ground movement; $S_{E,P}$ = Median photographic evidence-based ejecta-induced settlement; $S_{E,final}$ = Best final estimate of ejecta-induced settlement rounded to the nearest 5 mm; Final plus/minus values are also rounded to the nearest 5 mm.

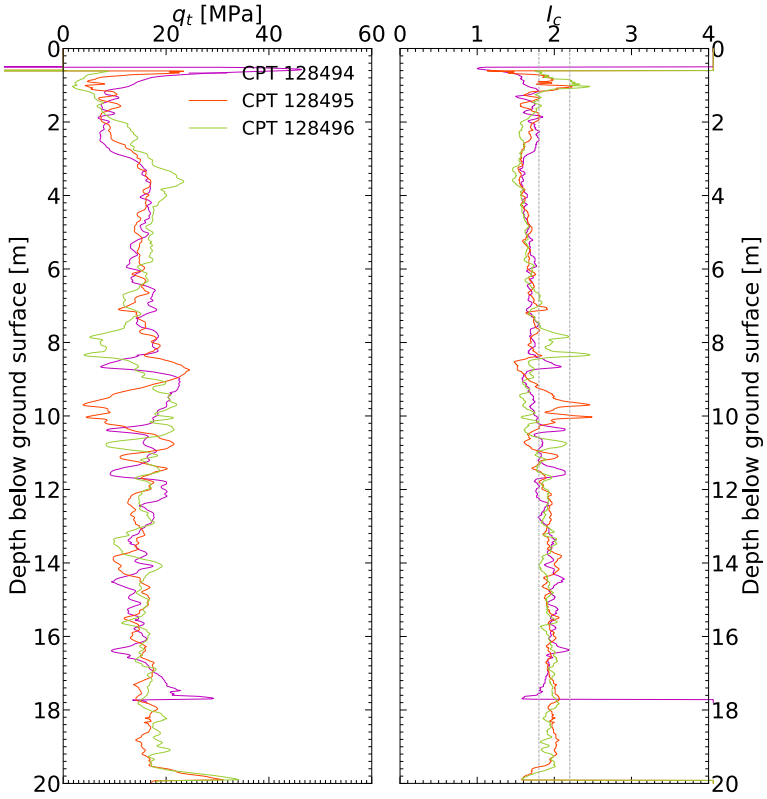

Figure 15: CPT traces for Tonks St.

Table 15: Ejecta-Induced settlement at the Tonks St site for the top 20 m of the soil profile for the 50th %ile PGA, P_L=50%, and C_{FC}=0.13 using BI-2014, ZRB-2002, and $I_{c,cutoff}$ of 2.6.

Earthquake Event(s)	M_W	PGA (g)	Depth to Groundwater (m)	S_{V1D} (mm)		
				10-m buffer	20-m buffer	50-m buffer
Sep 2010	7.1	0.19	3.3	0±20	1±20	1±20
Feb 2011	6.2	0.56	3.3	14±50	20±50	23±50
Jun 2011	6.2	0.22	2.5	0±25	1±25	1±25
Dec 2011	6.1	0.41	2.3	6±50	11±50	13±50

Notes: S_{V1D} = Average vertical settlement due to volumetric compression using Boulanger and Idriss (2014) (BI-2014), Zhang et al. (2002) (ZRB-2002) procedures and de Greef and Lengkeek (2018) thin-layer correction.

Table 16: CPT-based results for the Tonks St site.

		CPT ID		
EQ Event	Parameter	128494	128495	128496
Sep 2010	S_{V1D} (mm)	0	2	1
	LSN	0	0	0
	LPI	0	0	0
	LPI_{ish}	0	0	0
	$D_{FS<1}$ (m)	undet.	undet.	undet.
Feb 2011	S_{V1D} (mm)	14	25	31
	LSN	1	2	3
	LPI	1	2	3
	LPI_{ish}	0	1	1
	$D_{FS<1}$ (m)	8.52	9.40	7.70
Jun 2011	S_{V1D} (mm)	0	2	1
	LSN	0	0	0
	LPI	0	0	0
	LPI_{ish}	0	0	0
	$D_{FS<1}$ (m)	undet.	undet.	undet.
Dec 2011	S_{V1D} (mm)	6	16	17
	LSN	1	2	2
	LPI	0	1	1
	LPI_{ish}	0	1	1
	$D_{FS<1}$ (m)	undet.	9.50	7.75

Notes: $D_{FS<1}$ = Depth to the first liquefiable layer (FS_L<1) that is at least 200-mm thick, as determined by the Boulanger and Idriss (2016) liquefaction-triggering procedure (P_L=50%, C_{FC}=0.13, and $I_{c,cutoff}$ =2.6), and exported from *Cliq v.3.0.3.2*; undet. = the specified soil layer was not detected.

4. CONCLUSION

The liquefaction ejecta-induced free-field settlement at 61 sites in Christchurch was estimated for each of the four major Canterbury earthquakes (i.e., the Sep 2010, Feb 2011, June 2011, and Dec 2011 earthquakes) using the photographic evidence and the airborne LiDAR survey elevation points because direct measurements of ejected soil and the associated settlement were not available. The best final estimate of ejecta-induced settlement was provided typically as the weighted average of the two estimates. The methodology used to estimate the ejecta-induced free-field settlement for the four earthquakes was described. Its application to two sites illustrates how the detailed case histories included in Appendix were developed.

The *EjectaCaseHistories_FlatFile_2021.xlsx* spreadsheet that summarizes key characteristics of the 61 sites and the ejecta-induced settlement at each of these sites for the Sep 2010, Feb 2011, June 2011, and Dec 2011 earthquake is provided as an electronic supplement. The flat file also lists the sites from the "55 sites" dataset that were not considered for the ejecta-induced settlement analyses (e.g., due to lateral spreading) as well as the sites for which the best-final estimates of ejecta-induced settlement were provided but no detailed analyses were performed.

The photographic evidence-based approach for estimating the ejecta-induced settlement relies on high-resolution aerial photographs, ground photographs, and the detailed inspection notes for individual properties by the EQC LDAT comprised of engineers, engineering geologists, and engineering technicians. The area of a site covered with ejecta was measured approximately by utilizing the *Google Earth*^{TM} tools on the high-resolution aerial photograph supplied for each earthquake event. The height of ejecta, as the second component of the ejected soil volume, could not be measured directly but could be estimated with reasonable confidence based on ground photographs and detailed LDAT property inspection notes that had measurements of ejecta, when available. The uncertainty in estimating the height of ejecta was accounted for by providing a range of potential heights rather than a single value.

The LiDAR-based approach for estimating the ejecta-induced settlement made use of elevation points surveyed by airborne LiDAR prior to and after each major earthquake event (in July 2003, Sep 2010, Mar 2011, May 2011, Sep 2011, Feb 2012, and Oct 2015). The pre-earthquake and post-earthquake ground surface elevations were averaged in Global Mapper over the assessment area of a site and the difference between the two elevations was the earthquake-induced ground surface subsidence. The earthquake-induced ground surface subsidence was then adjusted for the vertical tectonic movement, artefacts of LiDAR (flight error bands), and global offset due to the median approximate error of each pre- and post-earthquake LiDAR survey relative to the GPS-surveyed benchmark points to obtain the liquefaction-induced ground settlement. The accuracy of the surveyed LiDAR elevation points was ±70 mm for all surveys except for the July 2003 survey that had the vertical accuracy of ±150 mm. The errors related to LiDAR measurements were accounted for and appended to each median/mean estimate, providing a range of liquefaction-induced settlement estimates. The estimated liquefaction-induced settlement had to be corrected further by removing the volumetric component. The volumetric-induced settlement was calculated using the available CPTs with the Zhang et al. (2002) procedure, and it was subtracted from the LiDAR-based liquefaction-induced settlement. The uncertainty associated with the Zhang et al. (2002) volumetric settlement for each earthquake event was estimated based on its sensitivity to the PGA, C_{FC}, and P_L. After the subtraction of the volumetric-induced settlement from the liquefaction-induced settlement, the ejecta-induced settlement was obtained.

The best final estimates of ejecta-induced settlement were calculated by assigning weights to each of the two estimated values described previously. This was done on a site-by-site basis, and it depended on site conditions, including the site's location relative to the LiDAR flight error bands, liquefaction performance of soil at the site relative to the estimations made by liquefaction-triggering procedures, and reasonableness of values estimated by the LiDAR. The LiDAR approach produced values that were at times inconsistent with the estimates generated by the photographic evidence approach. There were cases of negligible ejecta observed at the site as evidenced by the photographs, yet LiDAR-based values indicated significant ejecta-induced settlement. Additionally, the LiDAR approach in a few cases estimated ground uplift (i.e., negative ejecta-induced settlement), although accounting for the uncertainty of the estimate typically led to a reasonable settlement value being within range of estimated values.

Therefore, the aerial LiDAR can be a good means of estimating ground surface subsidence on a regional scale as was the case for Christchurch and its suburbs that were severely affected by the 2010-2011 Canterbury earthquakes, although one must be aware of the LiDAR-associated errors and account for them in the settlement analyses. However, for individual sites and detailed ejecta-induced settlement assessment, surveying elevation points via terrestrial LiDAR may be a better approach to avoid errors such as those associated with the LiDAR flights that can be on the

order of ±100 mm. This error becomes significant for individual sites that typically have the ground surface subsidence within the LiDAR margin of error. The LiDAR measurements are also affected by vegetation and topographic features such as undulations that appeared at many sites in Christchurch following the earthquakes. The uncertainty in the LiDAR-based approach can also be attributed to the vertical tectonic movements that resulted from each earthquake. These values for the analyzed sites were in a typical range from -100 mm to +100 mm. Subtracting the volumetric-induced settlement from the LiDAR-based liquefaction-induced settlement, further added to the uncertainty associated with the estimates of ejecta-induced settlement.

The photographic evidence provided generally more consistent results of ejecta-induced settlement, mainly due to the method's dependence on the area covered by ejecta, which could be obtained with reasonable confidence. Approximating geometrically the complex shapes of ejecta introduced some uncertainty; however, the greatest uncertainty in the method could be ascribed to estimating the height of ejecta, especially in the absence of ground photographs and detailed property inspection notes. At the time of the inspection, ejecta were often removed or ground photographs only showed traces of ejecta in places where large amounts of ejecta were observed in the high-resolution aerial photographs. Additionally, grass can obscure ejecta.

Nevertheless, the analyzed geotechnical database for the 2010-2011 Canterbury earthquakes provides a good set of data for developing detailed ejecta case histories. Rarely is there the wealth of data related to liquefaction-induced land damage like those for the 2010-2011 CES as few countries in earthquake-prone regions have residential land insured for damage from natural disasters. Also, rarely does a single site experience significant, repeated liquefaction and formation of ejecta under varying levels of ground motion in a short span of time, like the sites in Christchurch. Therefore, the detailed 244 case histories developed in this study constitute a unique database that can be used to examine the occurrence and effects of ejecta. The data provide a reasonable basis for the development of a procedure to evaluate when liquefaction ejecta will or will not occur and to estimate the quantity of ejecta in earthquakes.

Post-earthquake reconnaissance teams should take direct measurements of ejecta immediately after future earthquakes while all related evidence remains intact. This can be performed by utilizing a measuring tape, land surveying equipment and applications. Terrestrial LiDAR and photogrammetry can be used at individual sites to collect useful, reliable data. The volume of ejecta can also be measured simply by shoveling the ejected soil into a standard-size bucket. A reasonable number of sites affected by ejecta should first be identified on a high-resolution aerial photograph, which can be acquired quickly and cost effectively. The inspection teams can use individual property maps to add locations of ejecta and sketch their approximate shapes. Many high-quality ground photographs should be taken. Subsurface investigations such as CPT soundings, soil sampling, groundwater table measurements, shear wave and compressional wave velocity measurements, can be performed later at the sites. All the above in combination with reliable PGA estimates would provide an excellent set of data that can be interrogated and appended to the database developed in this study with an aim of developing a robust procedure for estimating the ejecta-induced settlement.

5. REFERENCES

Boulanger, R.W. and Idriss, I.M. (2014). "CPT and SPT Based Liquefaction Triggering Procedures." Report No. UCD/CGM-14/01. Center for Geotechnical Modeling, Dept. of Civil and Environmental Engineering, University of California, Davis.

Boulanger, R. W., & Idriss, I. M. (2016). CPT-Based Liquefaction Triggering Procedure. J. of Geotechnical and Geoenvironmental Engineering, 142(2), 04015065—1-11. doi: 10.1061/(asce)gt.1943-5606.0001388

Bradley, B., & Hughes, M. (2012). Conditional Peak Ground Accelerations in the Canterbury Earthquakes for Conventional Liquefaction Assessment. *Technical Report prepared for the Department of Building and Housing, New Zealand*.

Bray, J. D., and Dashti, S. (2014). Liquefaction-induced building movements. *Bulletin of Earthquake Engineering*, 12, 1129–56. doi.org/10.1007/s10518-014-9619-8

Bray, J.D. and Macedo, J. (2017). 6th Ishihara Lecture: Simplified Procedure for Estimating Liquefaction-Induced Building Settlement. *Soil Dynamics and Earthquake Engineering* J., V 102, 215-231.

Canterbury Geotechnical Database (2012a) "Aerial Photography", Map Layer CGD0100 - 1 June 2012, retrieved July 2018 – July 2021 from https://canterburygeotechnicaldatabase.projectorbit.com/

Canterbury Geotechnical Database (2012b) "Observed Ground Crack Locations", Map Layer CGD0400 - 23 July 2012, retrieved July 2018 – July 2021 from https://canterburygeotechnicaldatabase.projectorbit.com/

Canterbury Geotechnical Database (2012c) "Vertical Ground Surface Movements", Map Layer CGD0600 - 23 July 2012, retrieved July 2018 – July 2021 from https://canterburygeotechnicaldatabase.projectorbit.com/

Canterbury Geotechnical Database (2012d) "Cadastral Boundaries (2010)", Map Layer CGD5090 - 25 Sept 2012, retrieved July 2018 – July 2021 from https://canterburygeotechnicaldatabase.projectorbit.com/

Canterbury Geotechnical Database (2013a) "Liquefaction Interpreted from Aerial Photography", Map Layer CGD0200 - 11 Feb 2013, retrieved July 2018 – July 2021 from https://canterburygeotechnicaldatabase.projectorbit.com/

Canterbury Geotechnical Database (2013b) "Liquefaction and Lateral Spreading Observations", Map Layer CGD0300 - 11 Feb 2013, retrieved July 2018 – July 2021 from https://canterburygeotechnicaldatabase.projectorbit.com/

Canterbury Geotechnical Database (2014) "Event Specific Groundwater Surface Elevations", Map Layer CGD0800 - 10 June 2014, retrieved July 2018 – July 2021 from https://canterburygeotechnicaldatabase.projectorbit.com/

Canterbury Geotechnical Database (2015a) "LiDAR and Digital Elevation Models", Map Layer CGD0500 - 20 July 2015, retrieved July 2018 – July 2021 from https://canterburygeotechnicaldatabase.projectorbit.com/

Canterbury Geotechnical Database (2015b) "Conditional PGA for Liquefaction Assessment", Map Layer CGD5110 - 20 July 2015, retrieved July 2018 – July 2021 from https://canterburygeotechnicaldatabase.projectorbit.com/

Cox, S. C., van Ballegooy, S., Rutter, H. K., Harte, D. S., Holden, C., Gulley, A. K., Lacrosse, V., & Manga, M. (2021). Can artesian groundwater and earthquake-induced aquifer leakage exacerbate the manifestation of liquefaction? *Engineering Geology*, 281, 105982. doi.org/10.1016/j.enggeo.2020.105982

Cubrinovski, M., Bradley, B., Wotherspoon, L. M., Green, R., Bray, J., Wood, C., Pender, M., Allen, J., Bradshaw, A., Rix, G., Taylor, M., Robinson, K., Henderson, D., Giorgini, S., Ma, K., Winkley, A., Zupan, J., O'Rourke, T., DePascale, G., and Wells, D. (2011). Geotechnical aspects of the 22 February 2011 Christchurch Earthquake. *New Zealand Soc. for Earthquake Engineering B.,* 44(4), 205-226.

Cubrinovski, M., Rhodes, A., Ntritsos, N., and van Ballegooy, S. (2017). System response of liquefiable deposits. *In* Proceedings of the 3rd International Conference on Performance-based Design in Earthquake Geotechnical Engineering, Vancouver, BC, 16-19 July.

Cubrinovski, M., Rhodes, A., Ntritsos, N., & van Ballegooy, S. (2019). System response of liquefiable deposits. Journal of Soil Dynamics and Earthquake Engineering, 124, 212-229. doi: 10.1016/j.soildyn.2018.05.013

de Greef, J., & Lengkeek, H. J. (2018). Transition and thin layer corrections for CPT based liquefaction analysis. *Proceedings of the 4th International Symposium on Cone Penetration Testing (CPT'18)*, 21-22 June, 2018, Delft, The Netherlands.

GNS Science. (2021). *The most recent aftershock map*. Retrieved Aug 1, 2021, from https://www.gns.cri.nz/Home/Our-Science/Natural-Hazards-and-Risks/Recent-Events/Canterbury-quake/Recent-aftershock-map

Hutabarat, D., & Bray J.D. (2021). Effective Stress Analysis of Liquefiable Sites to Estimate the Severity of Sediment Ejecta. *J. of Geotechnical and Geoenvironmental Engineering, ASCE,* 10.1061/(ASCE)GT.1943-5606.0002503.

Ioannides, J. T. (2019). Cliq v.3.0.3.2 – CPT soil liquefaction software. Greece: Geologismiki.

Iwasaki, T., Arakawa, T. & Tokida, K. (1982). Simplified procedures for assessing soil liquefaction during earthquakes. *Conference on Soil Dynamics & Earthquake Engineering, Southampton*: 925-939.

Land Damage Assessment Team (LDAT). (2021). LDAT Reports Data Entry (Database). Retrieved from https://tracker.projectorbit.com/Sites/LDAT/EQCFieldReportFormExtra.aspx

Lees, J., van Ballegooy, S., & Wentz, F. J. (2015). Liquefaction susceptibility and fines content correlations of Christchurch soils. *6th International Conference on Earthquake Geotechnical Engineering*, 1-4 November 2015, Christchurch, New Zealand.

Maurer, B. W., Green, R. A., Cubrinovski, M., & Bradley, B. A. (2014). Evaluation of the Liquefaction Potential Index for Assessing Liquefaction Hazard in Christchurch, New Zealand. Journal of Geotechnical and Geoenvironmental Engineering, 140(7), 04014032-1-11. doi:10.1061/(asce)gt.1943-5606.0001117

Maurer, B., Green, R., van Ballegooy, S., & Wotherspoon, L. (2019). Development of region-specific soil behavior type index correlations for evaluating liquefaction hazard in Christchurch, New Zealand. Soil Dynamics and Earthquake Engineering, 117, 96-105.

Obermeier, S. F. (1996). Use of Liquefaction-Induced Features for Paleoseismic Analysis. *Engineering Geology*, 44, 1-76.

Quigley, M. C., Hughes, M. W., Bradley, B. A., van Ballegooy, S., Reid, C., Morgenroth, J., Horton, T., Duffy, B., and Pettinga, J. R. (2016). The 2010-2011 Canterbury Earthquake Sequence: Environmental effects, seismic triggering thresholds and geologic legacy. *Tectonophysics*, 672-673, 228–274. https://doi.org/10.1016/j.tecto.2016.01.044

Rogers, N., van Ballegooy, S., Williams, K., and Johnson, L. (2015). Considering post-disaster damage to residential building construction - Is our modern building construction resilient? *6th International Conference on Earthquake Geotechnical Engineering*, Christchurch, New Zealand.

Russell, J., and van Ballegooy, S. (2015). Canterbury Earthquake Sequence: Increased Liquefaction Vulnerability Assessment Methodology. *T+T Report 0028-1-R-JICR-2015 prepared for the Earthquake Commission.*

Stewart, J. P., Kramer, S. L., Kwak, D. Y., Greenfield, M. W., Kayen, R. E., Tokimatsu, K., Bray, J. D., Beyzaei, C. Z., Cubrinovski, M., Sekiguchi, T., Nakai, S., and Bozorgnia, Y. (2016). PEER-NGL Project: Open-Source Global Database and Model Development for the Next-Generation of Liquefaction Assessment Procedures. *Soil Dynamics and Earthquake Engineering* J., V. 91, 317-328.

Tonkin & Taylor Ltd. (T+T). (2013). *Liquefaction vulnerability study - Report to Earthquake Commission*. (Report 52020.0200) February 2013.

Tonkin and Taylor, Ltd. (2015). Tonkin and Taylor Geotechnical Database: Canterbury Maps (Database). Retrieved from https://canterburygeotechnicaldatabase.projectorbit.com/

van Ballegooy, S., S., Malan, P., Lacrosse, V., Jacka, M., Cubrinovski, M., Bray, J. D., O'Rourke, T. D., Crawford, S. A., and Cowan, H. (2014). Assessment of liquefaction-induced land damage for residential Christchurch. *Earthquake Spectra, 30*(1): 31-55.

Zhang, G., Robertson, P. K., and Brachman, R. W. I. (2002). Estimating Liquefaction-Induced Ground Settlements from CPT for Level Ground. *Can. Geotech. J.*, 39, 1168-1180. doi: 10.1139/T02-047

6. APPENDIX A – DETAILED CASE HISTORIES

The PDF file with the detailed case histories can be found here:
https://berkeley.box.com/s/4jd5htgri4l60pr25hc32m3wifsqtf7x.

7. APPENDIX B – FLAT FILE

The Excel file with the ejecta-induced settlement estimates and other key information for each case history can be found here:
https://berkeley.box.com/s/3wi2ev7pocmdbc3i79ri55svr3ubwxet.